AMERICAN SOCIETY FOR MICROBIOLOGY | Journal of Virology

Host-Microbial Interactions | Full-Length Text

# Essential role of the CCL2–CCR2 axis in Mayaro virus-induced disease

**Franciele Martins Santos,[1] Victor Rodrigues de Melo Costa,[1] Simone de Araújo,[2] Carla Daiane Ferreira de Sousa,[3] Thaiane Pinto Moreira,[3] Matheus Rodrigues Gonçalves,[1] Anna Clara Paiva Menezes dos Santos,[3] Heloísa Athayde Seabra Ferreira,[2] Pedro Augusto Carvalho Costa,[2] Breno Rocha Barrioni,[4] Paula Bargi-Souza,[2] Marivalda de Magalhães Pereira,[4] Maurício Lacerda Nogueira,[5] Danielle da Glória Souza,[3] Pedro Pires Goulart Guimarães,[2] Mauro Martins Teixeira,[6] Celso Martins Queiroz-Junior,[1] Vivian Vasconcelos Costa[1]**

**AUTHOR AFFILIATIONS** See affiliation list on p. 21.

**ABSTRACT** Mayaro virus (MAYV) is an emerging arbovirus member of the *Togaviridae* family and *Alphavirus* genus. MAYV infection causes an acute febrile illness accompanied by persistent polyarthralgia and myalgia. Understanding the mechanisms involved in arthritis caused by alphaviruses is necessary to develop specific therapies. In this work, we investigated the role of the CCL2/CCR2 axis in the pathogenesis of MAYV-induced disease. For this, wild-type (WT) C57BL/6J and CCR2$^{-/-}$ mice were infected with MAYV subcutaneously and evaluated for disease development. MAYV infection induced an acute inflammatory disease in WT mice. The immune response profile was characterized by an increase in the production of inflammatory mediators, such as IL-6, TNF, and CCL2. Higher levels of CCL2 at the local and systemic levels were followed by the significant recruitment of CCR2$^{+}$ macrophages and a cellular response orchestrated by these cells. CCR2$^{-/-}$ mice showed an increase in CXCL-1 levels, followed by a replacement of the macrophage inflammatory infiltrate by neutrophils. Additionally, the absence of the CCR2 receptor protected mice from bone loss induced by MAYV. Accordingly, the silencing of CCL2 chemokine expression *in vivo* and the pharmacological blockade of CCR2 promoted a partial improvement in disease. Cell culture data support the mechanism underlying the bone pathology of MAYV, in which MAYV infection promotes a pro-osteoclastogenic microenvironment mediated by CCL2, IL-6, and TNF, which induces the migration and differentiation of osteoclast precursor cells. Overall, these data contribute to the understanding of the pathophysiology of MAYV infection and the identification future of specific therapeutic targets in MAYV-induced disease.

**IMPORTANCE** This work demonstrates the role of the CCL2/CCR2 axis in MAYV-induced disease. The infection of wild-type (WT) C57BL/6J and CCR2$^{-/-}$ mice was associated with high levels of CCL2, an important chemoattractant involved in the recruitment of macrophages, the main precursor of osteoclasts. In the absence of the CCR2 receptor, there is a mitigation of macrophage migration to the target organs of infection and protection of these mice against bone loss induced by MAYV infection. Much evidence has shown that host immune response factors contribute significantly to the tissue damage associated with alphavirus infections. Thus, this work highlights molecular and cellular targets involved in the pathogenesis of arthritis triggered by MAYV and identifies novel therapeutic possibilities directed to the host inflammatory response unleashed by MAYV.

**KEYWORDS** Mayaro virus, alphavirus, CCR2 receptor, CCL2 chemokine, bone loss, inflammation

**Editor** Mark T. Heise, University of North Carolina at Chapel Hill, Chapel Hill, North Carolina, USA

Address correspondence to Celso Martins Queiroz-Junior, cmqj@ufmg.br, or Vivian Vasconcelos Costa, vivianvcosta@gmail.com.

The authors declare no conflict of interest.

See the funding table on p. 22.

**Received** 20 July 2023
**Accepted** 2 December 2023
**Published** 3 January 2024

Mayaro virus (MAYV) is an endemic arthritogenic arbovirus that is widely neglected in South and Central American countries. MAYV belongs to the *Togaviridae* family and the genus *Alphavirus*, which also includes Chikungunya (CHIKV), Ross River (RRV), and Sindbis viruses. These viruses are enveloped and have a positive-polarity single-stranded RNA genome (1). MAYV is responsible for sporadic outbreaks of acute febrile illness, particularly in regions around the Amazon basin where it is maintained in wild and rural cycles. *Haemagogus* mosquitoes and non-human primates are considered the main vectors and hosts, respectively (2).

Mayaro fever (MF) is clinically characterized by fever, rash, retro-orbital pain, headache, arthralgia, and myalgia. As with CHIKV infection, highly debilitating and persistent arthralgia is a hallmark of MAYV infection, which primarily affects the joints of the wrists, elbows, knees, and small joints of the hands and feet (3–6). Persistent arthralgia occurs in more than 50% of MF cases, which can last from months to years, resulting in a large socioeconomic impact (3). The mechanisms associated with MAYV arthralgia pathogenesis are poorly understood. Meanwhile, host inflammatory immune responses seem to play a key role in the development and progression of alphavirus-induced diseases (7).

Macrophages and their pro-inflammatory products, such as CCL2, TNF, and INF-γ, are considered the main critical factors in the development of RRV and CHIKV-induced myositis and arthritis (8–10). Additionally, IL-6 and the chemokines CCL2, CCL8, and CCL7 have been reported to be involved in osteoclastogenesis during alphaviral infections (11, 12). Accordingly, a recently proposed animal model for MAYV has shown that MAYV infection induces significant inflammatory responses mediated by TNF, IL-6, INF-γ, and CCL2, similar to other alphaviruses (13). Noteworthy, elevated CCL2 levels have been detected in the synovial fluid of patients infected with RRV and CHIKV (14, 15) as well as in the serum of patients with MF during the acute phase of the disease (16).

The CCL2–CCR2 axis is responsible for modulating monocyte/macrophage recruitment in several chronic inflammatory diseases including atherosclerosis, cancer, and arthritis (17). In inflammatory sterile conditions such as rheumatoid arthritis (RA) and osteoarthritis (OA), elevated CCL2 levels were detected in the blood, synovial fluid, and synovial tissue of patients. Furthermore, studies in animal models of osteoarthritis have demonstrated that the CCL2/CCR2 pathway is primarily responsible for the recruitment of monocytes and the establishment of pain and associated tissue damage (18–20). Accordingly, in infectious arthritis models, such as the one induced by CHIKV, CCR2 knockout mice presented more severe arthritis that was associated with an intense neutrophil infiltrate. In contrast, the inhibition of CCL2 was associated with a reduction in arthritis, myositis, and bone loss in mice infected with CHIKV and RRV (12, 21).

Thus, the aim of the present study was to investigate the role of the CCL2/CCR2 axis in the pathogenesis of MAYV-induced disease. Our results demonstrated that MAYV induced an acute inflammatory disease, characterized by local edema, hypernociception, and myositis in wild-type (WT) and $CCR2^{-/-}$ mice. Meanwhile, viral load analysis revealed a reduction in viable virus titers in most organs analyzed from $CCR2^{-/-}$ mice. Interestingly, in the absence of CCL2/CCR2 signaling, bone tissue homeostasis was only slightly affected during MAYV infection. *In vitro*, our data support the mechanism underlying the bone pathology of MAYV, in which the infection promotes a pro-osteoclastogenic microenvironment mediated by the production of IL-6, TNF, and CCL2, which consequently induces the migration of osteoclast precursors.

## RESULTS

### Characterization of MAYV-induced disease in C57BL/6J mice

First, a characterization of the MAYV-induced disease in young C57BL/6J mice was performed. To that end, 4-week-old mice were infected in the right hind paw with $1 \times 10^6$ PFU of MAYV, and signs of disease, including hypernociception, viral loads in several organs, and tissue damage during the course of infection, were evaluated. MAYV induced significant hind paw edema and reduced the nociceptive threshold as early as 1 day

post-infection (PI) (Fig. 1A and B). Hind paw edema peaked at day 5 PI and persisted for up to 15 days PI (Fig. 1A). Meanwhile, the nociceptive threshold remained low for up to 28 days upon MAYV inoculation, returning to baseline levels at day 35. These clinical signs were associated with significant inflammatory damage in hind paw tissues (Fig.

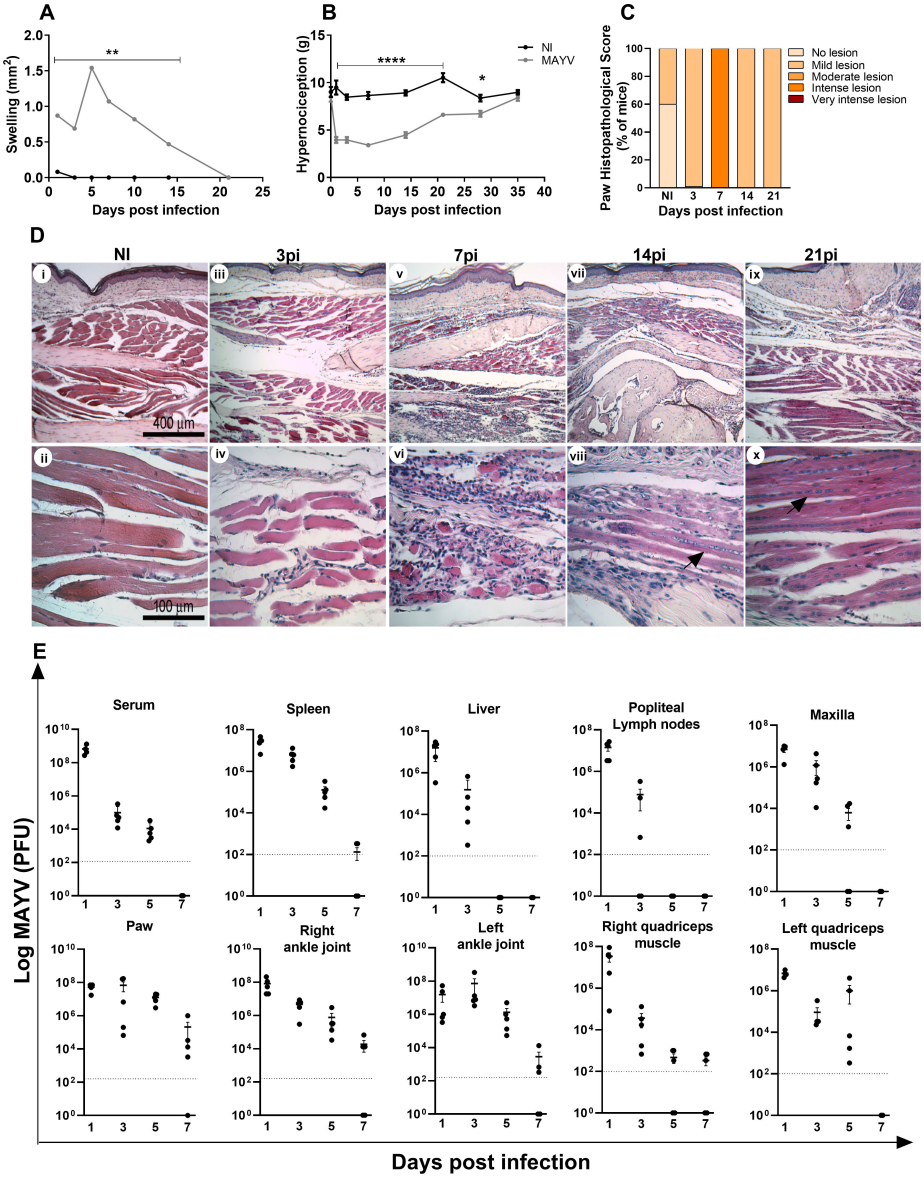


**FIG 1** MAYV-induced disease in C57BL/6J mice. Four-week-old mice were infected through the rear right footpad with 30 µL containing $10^6$ PFU of MAYV or were mock-infected with phosphate-buffered saline (PBS) 1×. (A) Edema measurements were performed in the infected paw (right paw) with the aid of a caliper. (B) Hypernociception threshold assessment was performed using the adapted von Frey method. Statistics were performed with two-way analysis of variance (ANOVA) and Tukey's multiple comparisons test ($^{*}P \leq 0.05$; $^{**}P < 0.0012$; $^{****}P < 0.0001$). (C) Histopathological score comprising inflammatory muscle damage. At days 3, 7, 14, and 21 PI, mice were euthanized, ankle tissues were removed and paraffin-embedded, and 5 µm sections were generated and stained with hematoxylin and eosin (H&E). Each mouse sample received a score as follows: no lesion (0), mild lesion (1 and 2), moderate lesion (3 and 4), intense lesion (5 and 6), and very intense lesion (7). Panel D shows negative control (i and ii) and MAYV infection at day 3 PI (iii and iv), day 7 PI (v and vi), day 14 PI (vii and viii), and day 21 PI (ix and x). Dark arrows indicate regenerating muscle fibers. Images i, iii, v, vii, and ix (100× magnification, 400 µm bar); images ii, iv, vi, viii, and x (400× magnification, 100 µm bar). (E) At days 1, 3, 5, and 7 PI, the serum and tissues of interest were harvested and homogenized, and the titers of infectious virus were determined by the plaque assay on Vero cells. Data are derived from at least five mice per group (mean ± SEM).

1C and D). Indeed, MAYV induced infiltration of inflammatory cells to the site of the infection, which is associated with myositis and loss of tissue architecture especially at day 7 PI (Fig. 1C and D, v and vi). At days 14 and 21 PI, there was still the presence of inflammatory infiltrate, but the onset of tissue recovery was already evident, as indicated by the presence of regenerating muscle fibers (Fig. 1D, viii and x). Accordingly, MAYV infected, replicated, and spread to different tissues, including the contralateral ankle joint and quadriceps femoris muscle, persisting significantly in ankle joints, right quadriceps, and paw for up to 7 days PI (Fig. 1E).

MAYV infection induced a marked increase in local (Fig. 2A) and systemic (Fig. 2E through H) CCL2 levels, which remained high up to 14 days PI in the paw, maxilla, quadriceps muscle, and spleen. The CCL5 chemokine was detected in quadriceps and paw tissues (Fig. 2B and I). The levels of the pro-inflammatory cytokines IL-6 and TNF increased only in the footpad at day 7 PI (Fig. 2C and D).

## The CCL2/CCR2 axis plays an important role in the development of MAYV-induced disease

To understand the role of the CCL2/CCR2 axis in the pathogenesis of MAYV, 4-week-old WT and CCR2$^{-/-}$ mice were infected with MAYV to evaluate disease development.

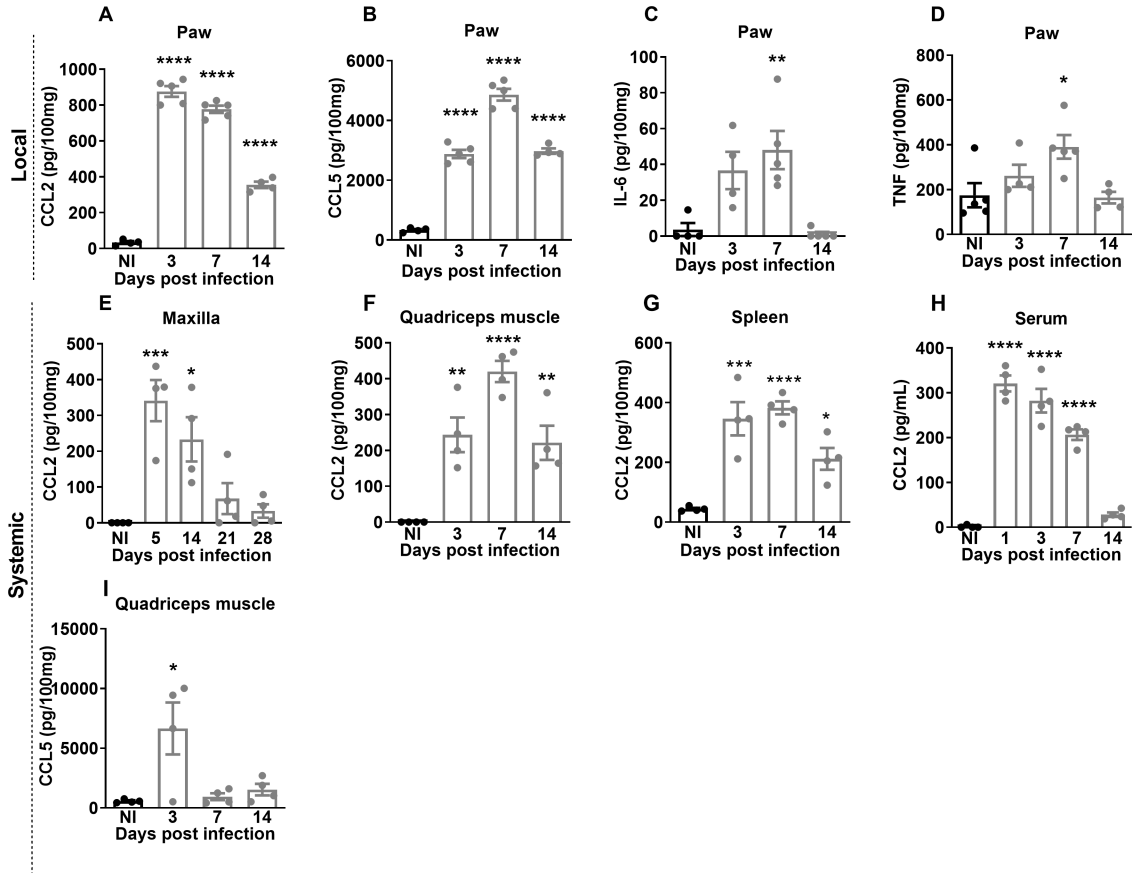


**FIG 2** MAYV induces the production of local and systemic inflammatory mediators in C57BL/6J mice. Four-week-old WT mice were infected through the right hind paw with $10^6$ PFU of MAYV. The NI group was injected with 1× PBS. On days 3, 7, and 14 PI, the paws were collected and processed for analysis of the local cytokine profile. The paw samples showed high levels of chemokines CCL2 (A) and CCL5 (B) and inflammatory cytokines IL-6 (C) and TNF (D). For the analysis of the systemic profile of cytokines and chemokines, the quadriceps muscle, serum, and spleen were collected on days 3, 7, and 14 PI, and the maxilla was collected on days 5, 14, 21, and 28 PI. The presence of CCL2 chemokines was detected in the maxilla (E), quadriceps muscle (F), spleen (G), and serum (H) and CCL5 in the quadriceps muscle (I). Statistics were performed with one-way ANOVA and Tukey's multiple comparisons test ($^{*}P$-value ≤0.05; $^{**}P$-value <0.01; $^{***}P$-value <0.001; $^{****}P$-value <0.0001). The asterisk indicates the difference between the time points of the infection kinetics and the uninfected group (NI). Data are derived from at least four mice per group (mean ± SEM).

Differently from what was observed in WT animals, CCR2$^{-/-}$ mice presented delayed paw edema, peaking at day 10 PI (Fig. 3A). The hypernociception threshold reduced in both WT and CCR2$^{-/-}$ infected mice at day 3 PI (Fig. 3B), with no difference between the groups. However, from the seventh day PI on, CCR2$^{-/-}$ animals recovered and returned to their baseline levels, while WT animals recovered to baseline levels at day 21 PI. As seen in WT animals, MAYV was also detected in the serum and various organs and tissues of the CCR2$^{-/-}$ mice. However, viral titers were significantly lower than in WT in all tissues analyzed. Interestingly, in the right and left ankle joints on day 7 PI, there was viral recovery above the limit of detection only in CCR2$^{-/-}$ mice (Fig. 3C and D). MAYV-induced inflammation in CCR2$^{-/-}$ mice started at 3 days PI, with the peak on the 7th and 14th days post-virus inoculation (Fig. 4A, vii–ix and 4B, ). Comparing to WT mice (ii–v), the inflammatory process was less intense in CCR2$^{-/-}$ animals (vii–x). On the other hand, it persisted longer in the CCR2$^{-/-}$ mice (Fig. 4A, vii–x), as the presence of degenerating fibers and myophagocytosis was still observed at days 14 and 21 post-MAYV inoculation (Fig. 4A, ix and x). Tissue recovery started at 21 days PI with the reduction of inflammatory cells and regeneration of injured tissue, whereas in WT animals, this tissue recovery started earlier with 14 days PI (Fig. 4A, iv and x).

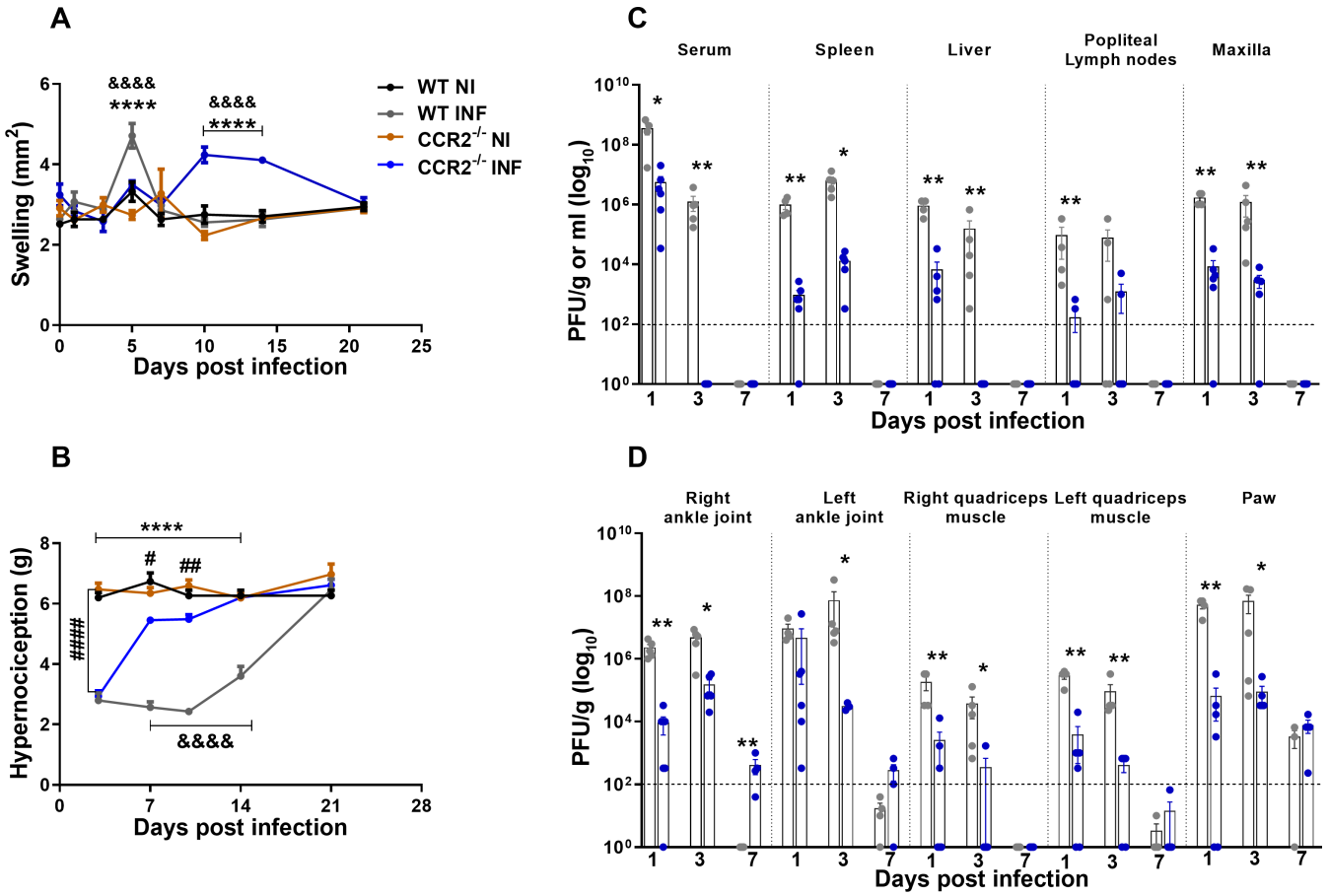


**FIG 3** MAYV Infection in CCR2$^{-/-}$ mice. Four-week-old WT and CCR2$^{-/-}$ mice (C57BL6 background) were infected via the rear right footpad with $10^6$ PFU of MAYV. The mock group was inoculated with PBS 1×. (A) Plantar edema measurement. Edema was measured with a caliper on the infected paw on 0, 1, 3, 5, 7, 10, 14, and 21 days PI. (B) Measurement of the hypernociception threshold. Statistics were performed with two-way ANOVA and Tukey's multiple comparisons test ($^{*}$*P*-value ≤0.05; $^{**}$*P*-value <0.01; $^{***}$*P*-value <0.001; $^{****}$*P*-value <0.0001). $^{*}$Difference between WT INF and WT NI; $^{\#}$difference between CCR2$^{-/-}$ INF and CCR2$^{-/-}$ NI; $^{\&}$difference between WT and CCR2$^{-/-}$. (C and D) At 1, 3, and 7 days PI, serum and tissues of interest were harvested and homogenized, and the titers of infectious virus were determined by the plaque assay on Vero cells. Statistics were performed with the Student *t*-test at each time point ($^{*}$*P*-value ≤0.05; $^{**}$*P*-value <0.01; $^{***}$*P*-value <0.001; $^{****}$*P*-value <0.0001). $^{*}$Difference between WT and CCR2$^{-/-}$. Data are derived from at least five mice per group (mean ± SEM).

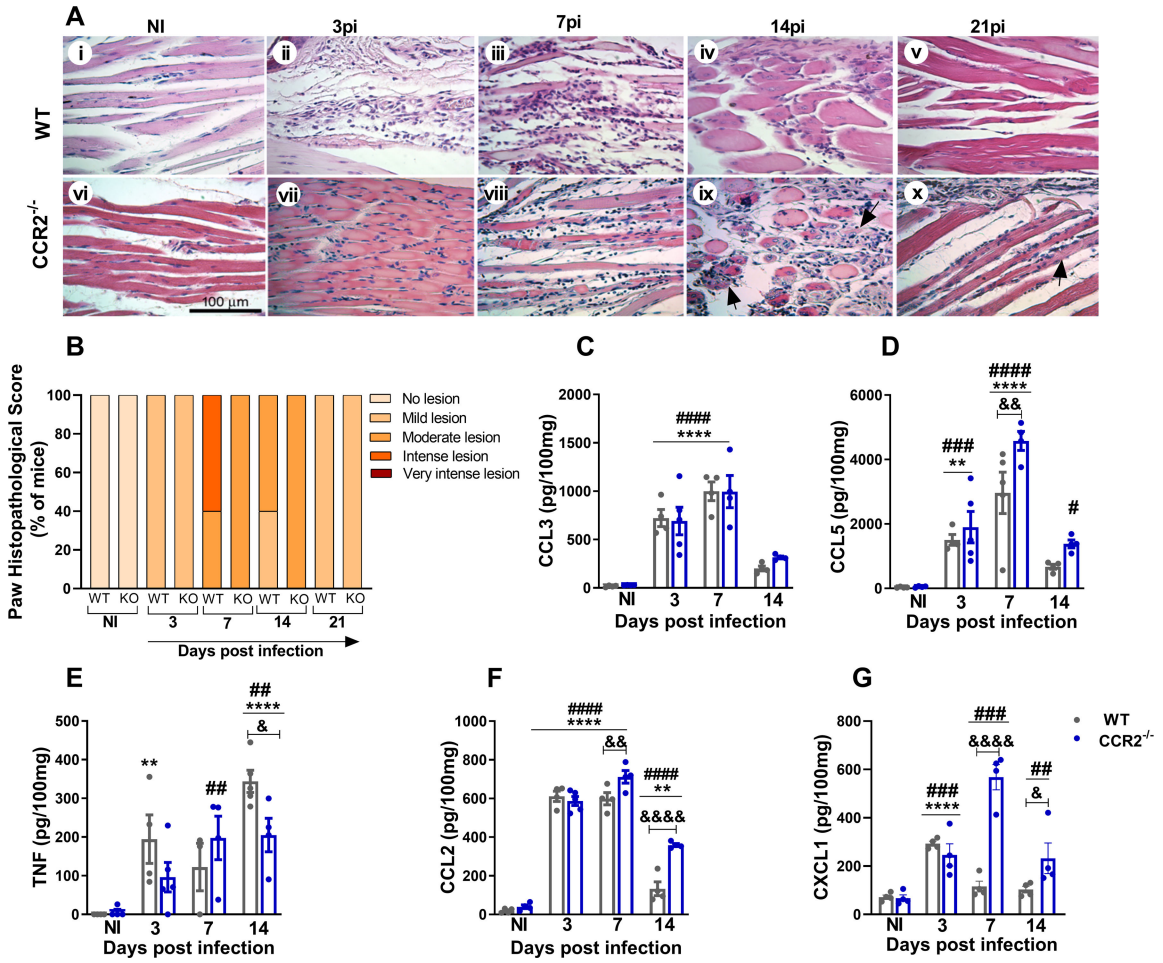


**FIG 4** MAYV induces moderate and prolonged inflammation in CCR2$^{-/-}$ mice. (A) At 3, 7, 14, and 21 days PI, mice were euthanized, ankle tissues were removed and paraffin-embedded, and 5-µm sections were generated and stained with H&E. Images i–x (400× magnification, 100 µm bar). (i–v) Panels show WT negative control (i) and MAYV infection at 3 (ii), 7 (iii), 14 (iv), and 21 (v) days PI. Corresponding endpoints are shown for CCR2$^{-/-}$ samples (vi–x). Black arrows indicate suggestive areas of myophagocytosis, as denoted by degenerating muscle fibers surrounded by leukocytes. (B) Paw histopathological score. No lesion (0), mild lesion (1 and 2), moderate lesion (3 and 4), intense lesion (5 and 6), and very intense lesion (7). (C–G) Kinetics of expression of the inflammatory mediators CCL3 (C), CCL5 (D), TNF (E), CCL2 (F), and CXCL1 (G) in the mice's paws on days 3, 7, and 14 PI. Statistics were performed with two-way ANOVA, followed by Tukey's multiple comparisons test ($^{*}P$-value ≤0.05; $^{**}P$-value <0.01; $^{***}P$-value <0.001; $^{****}P$-value <0.0001). $^{*}$Difference between WT INF and WT NI; $^{\#}$difference between CCR2$^{-/-}$ INF and CCR2$^{-/-}$ NI; $^{\&}$difference between WT and CCR2$^{-/-}$. Data are derived from at least four mice per group (mean ± SEM).

Our results so far demonstrate that MAYV-infected CCR2$^{-/-}$ mice present reduced clinical and histological signs of inflammation (Fig. 3A, B, 4A and B). Regarding inflammatory mediators in the paw, no significant differences in the expression kinetics of CCL3 (Fig. 4C) were observed when comparing WT versus CCR2$^{-/-}$ mice. Meanwhile, CCL5 levels increased at 7 days PI (Fig. 4D); TNF levels reduced at 14 days PI (Fig. 4E), while CCL2 levels were higher at days 7 and 14 PI in knockout than WT mice (Fig. 4F). Interestingly, the chemokine CXCL-1, a promoter of neutrophil recruitment, was significantly elevated at days 7 and 14 PI in knockout mice compared to WT animals (Fig. 4G).

## MAYV-induced bone resorption in WT versus CCR2$^{-/-}$ mice

The inflammatory response induced by MAYV infection was characterized by a significant pro-osteoclastogenic milieu, as demonstrated by the increased local expression of IL-6, TNF, and CCL2 and systemic overexpression of CCL2. To assess the impact of MAYV infection on bone tissue, samples of tibia were submitted to microtomography [micro-CT

(μCT)] analysis at 21 days PI. Bone parameter data comparing WT and CCR2$^{-/-}$ mice were expressed as delta (infected sample minus non-infected mean) to eliminate the bias of the baseline difference in bone mass that exists between these animals. MAYV induced significant bone loss in the distal tibial metaphysis region of WT mice, in contrast to CCR2$^{-/-}$ mice (Fig. 5). There was a significant reduction in bone volume (Fig. 5A) in the tibia of WT infected mice, as well as in the trabecular number (Fig. 5B), accompanied by an increase in the porosity (Fig. 5C and F, i and ii). In contrast, bone homeostasis in CCR2$^{-/-}$ animals was not affected by MAYV infection. There was no significant bone resorptive phenotype in the tibia of CCR2$^{-/-}$ mice, as indicated by the BV/TV, Po, and Tb.Sp delta values close to zero (Fig. 5A through D and F).

To confirm the increase in bone resorption activity in the tibia, we performed TRAP staining, an enzyme expressed by osteoclasts during bone resorption. The number of TRAP$^{+}$ cells was significantly increased in WT-infected animals, while CCR2$^{-/-}$ mice, despite the increased number of TRAP$^{+}$ cells in the basal condition, did not present higher numbers after infection (Fig. 5E). These data indicate that the CCR2 receptor contributes to the bone resorptive phenotype observed during MAYV infection.

## Absence of CCR2 resulted in a shift of mononuclear infiltrate to polymorphonuclear cells during MAYV infection

To determine the pattern of the cellular immune response against MAYV infection, WT and CCR2$^{-/-}$ immune cells were isolated from the hind paw, and the cellular profile was evaluated by flow cytometry. To create the Boolean gate, debris were excluded through the combinations of fluorochromes. For the remotion of doublets, a forward scatter area (FSC-A) versus forward scatter height gate was used, and then, cells were gated in the function of time versus FSC-A to avoid a possible interference of flux interruptions. MAYV infection increased the frequency in myeloid cells in both infected groups on day 7 PI, with a greater increase in the WT group (Fig. 6A and B). At day

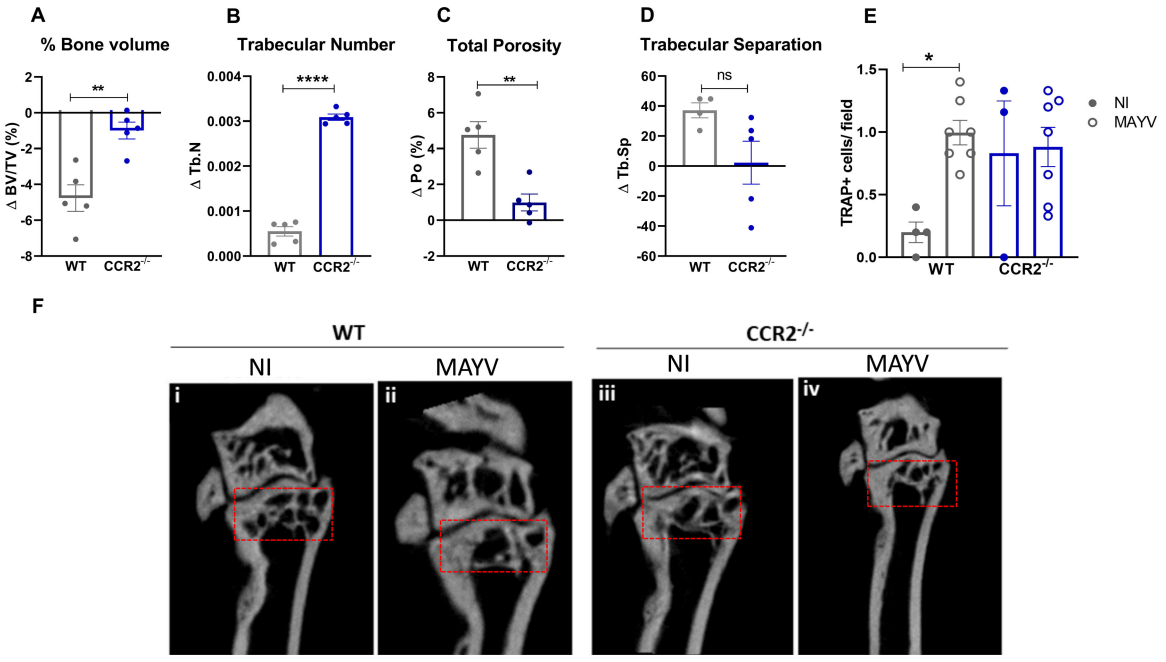


**FIG 5** CCR2$^{-/-}$ mice are resistant to bone resorption induced by MAYV. Four-week-old WT and CCR2$^{-/-}$ mice (C57BL/6J background) were infected via the rear right footpad with $10^6$ PFU of MAYV. The mock group was inoculated with PBS 1×. At day 21 PI, animals were euthanized, and the tibia was removed for micro-CT analysis. (A) Trabecular bone volume fraction [BV/TV (%)], (B) trabecular number (Tb.N), (C) porosity in the tibia [Po (%)], and (D) trabecular separation (Tb.Sp). Statistics were performed with Student's unpaired *t*-test (**$P$-value <0.01). Data are derived from at least four mice per group. (E) Number of tartrate-resistant acid phosphatase-positive (TRAP$^{+}$) cells detected in the distal tibial metaphysis region per microscopic 400× field. Statistics were performed with one-way ANOVA, followed by Tukey's multiple comparisons test (*$P$-value <0.05). (F) 2D reconstruction of the distal tibia samples. Red box, region of analysis.

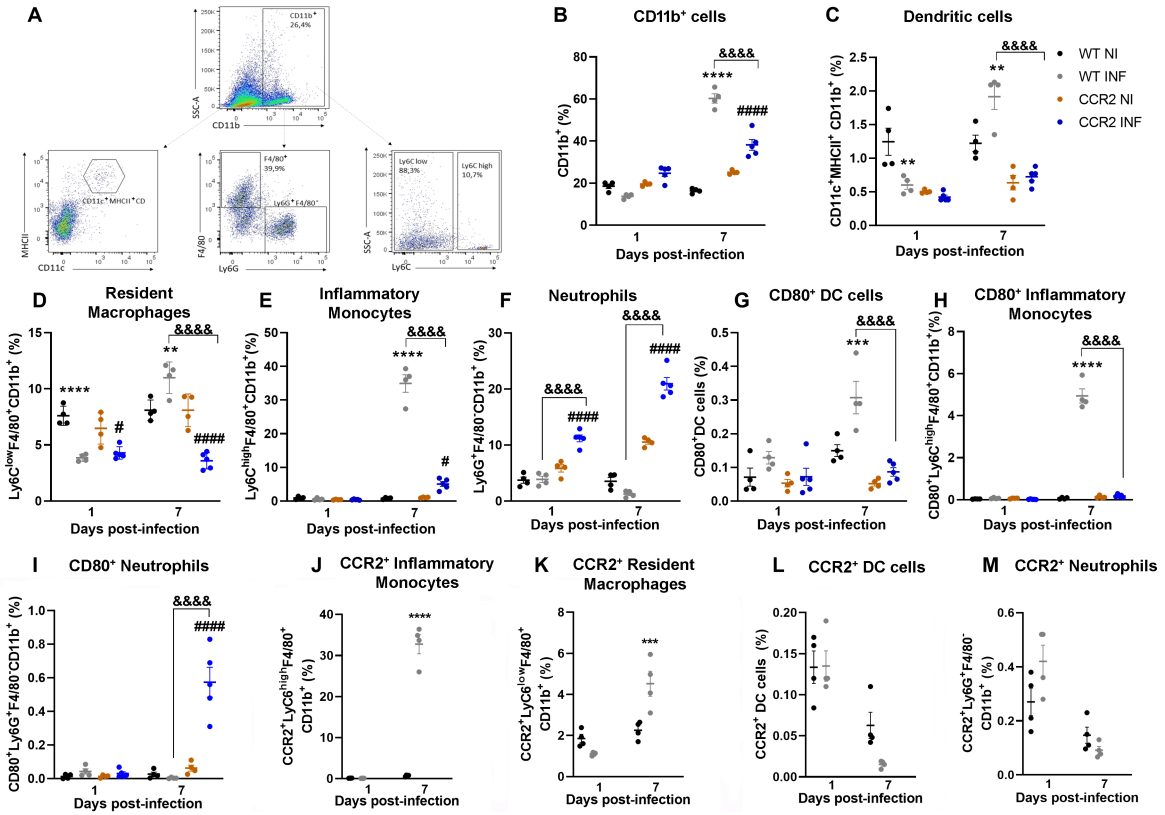


**FIG 6** Profile of myeloid immune cells in the paw of MAYV-infected WT and CCR2$^{-/-}$ mice. Flow cytometry analysis of immune cells isolated from the hind paw of animals infected with MAYV at days 1 and 7 PI. (A) The panel shows the gating strategy for defining the population of myeloid cells from the single cells. % of total cells were used to represent myeloid cell subsets. (B) Increase of CD11b$^+$ cells at 7 days PI in WT and CCR2$^{-/-}$ animals. (C) Percentage of dendritic cells (CD11c$^+$MHCII$^+$CD11b$^+$). (D) Percentage of resident macrophages (Ly6C$^{low}$F4/80$^+$CD11b$^+$). (E) Percentage of inflammatory monocytes (Ly6C$^{high}$F4/80$^+$CD11b$^+$). (F) Percentage of neutrophils (Ly6G$^+$F4/80$^-$CD11b$^+$). (G) Percentage of dendritic cells expressing CD80. (H) Percentage of inflammatory monocytes expressing CD80. (I) Percentage of neutrophils expressing CD80. Percentage of inflammatory monocytes (J), macrophages (K), dendritic cells (L), and neutrophils (M) expressing CCR2. Statistics were performed with two-way ANOVA, followed by Tukey's multiple comparisons test ($^*$*P*-value ≤0.05; $^{**}$*P*-value <0.01; $^{***}$*P*-value <0.001; $^{****}$*P*-value <0.0001). $^*$Difference between WT NI and WT INF; $^\#$difference between CCR2$^{-/-}$ NI and CCR2$^{-/-}$ INF; $^\&$difference between WT and CCR2$^{-/-}$. Data are derived from at least five mice per group (mean ± SEM).

1 PI, WT mice showed a reduction in the population percentage of dendritic cells (CD11c$^+$MHCII$^+$CD11b$^+$) and resident macrophages (Ly6C$^{low}$F4/80$^+$CD11b$^+$) (Fig. 6C and D). WT mice showed a response mainly characterized by monocytes/macrophages, which are suggested to be the main cell population involved in alphaviral pathogenesis (13). An increase in the percentage of inflammatory monocytes (Ly6C$^{high}$F4/80$^+$CD11b$^+$) was observed 7 days after MAYV inoculation (Fig. 6E), and approximately 30% of these cells were CCR2$^+$ monocytes (Fig. 6J). Finally, a twofold increase in the population percentage of dendritic cells and resident macrophages (Ly6C$^{low}$F4/80$^+$CD11b$^+$) was observed at day 7 PI (Fig. 6C and D), and approximately 50% of these macrophages are CCR2$^+$ (Ly6C$^{low}$CCR2$^+$) (Fig. 6K). Interestingly, no significant increase in the percentage of neutrophils (Ly6G$^+$F4/80$^-$CD11b$^+$) was observed in WT animals after the inoculation of MAYV (Fig. 6F). Furthermore, the populations of dendritic cells and neutrophils analyzed were not characterized by a relevant presence of CCR2$^+$ cells (Fig. 6L and M), as observed in the populations of macrophages and monocytes on day 7 post-infection. Finally, the activation state of these myeloid cell populations was confirmed by cell surface molecule CD80 on monocytes and dendritic cells (Fig. 6G through I).

On the other hand, cellular responses of CCR2$^{-/-}$ mice were characterized by a reduced population of infiltrating inflammatory monocytes/macrophages (Fig. 6E), which was replaced by a significant increase in the percentage of neutrophils, observed

on days 1 and 7 after MAYV inoculation (Fig. 6F). Furthermore, the activation status of these neutrophil population was confirmed by an increase in the percentage of CD80-positive cells at day 7 PI (Fig. 6I). Finally, both infected groups revealed an increased percentage of $CD4^+$ and $CD8^+$ lymphocytes at 7 days PI (Fig. 7A through D), while $CCR2^{-/-}$ mice showed a higher percentage of $CD4^+$ T cells in comparison to WT. Consequently, the activation marker analysis showed an increase in the percentage of $CD4^+$ and $CD8^+$ T cells positive for CD69 and CD44 markers in both infected groups, while $CCR2^{-/-}$ mice showed a higher percentage of these cells than WT mice (Fig. 7E, F, H, and I). Interestingly, an increase in the percentage of T cells $CD44^+/CD62L^+$, a marker for memory cells, was observed exclusively in WT (Fig. 7G and J) mice. Furthermore, we observed a significant presence of $CCR2^+$ T cells in the inflammatory infiltrate of WT mice at 7 days PI (Fig. 7K and L).

Overall, these data show that during MAYV infection, the CCR2 receptor directs the influx and activation of monocytes to the site of infection, which negatively affects the course and severity of the disease. Meanwhile, in the absence of the CCR2 receptor, a differential cellular pattern of cellular infiltration occurs characterized by the presence of neutrophils. This replacement of monocytes by neutrophils in $CCR2^{-/-}$ mice may largely explain the improvement observed in important parameters of the disease, such as

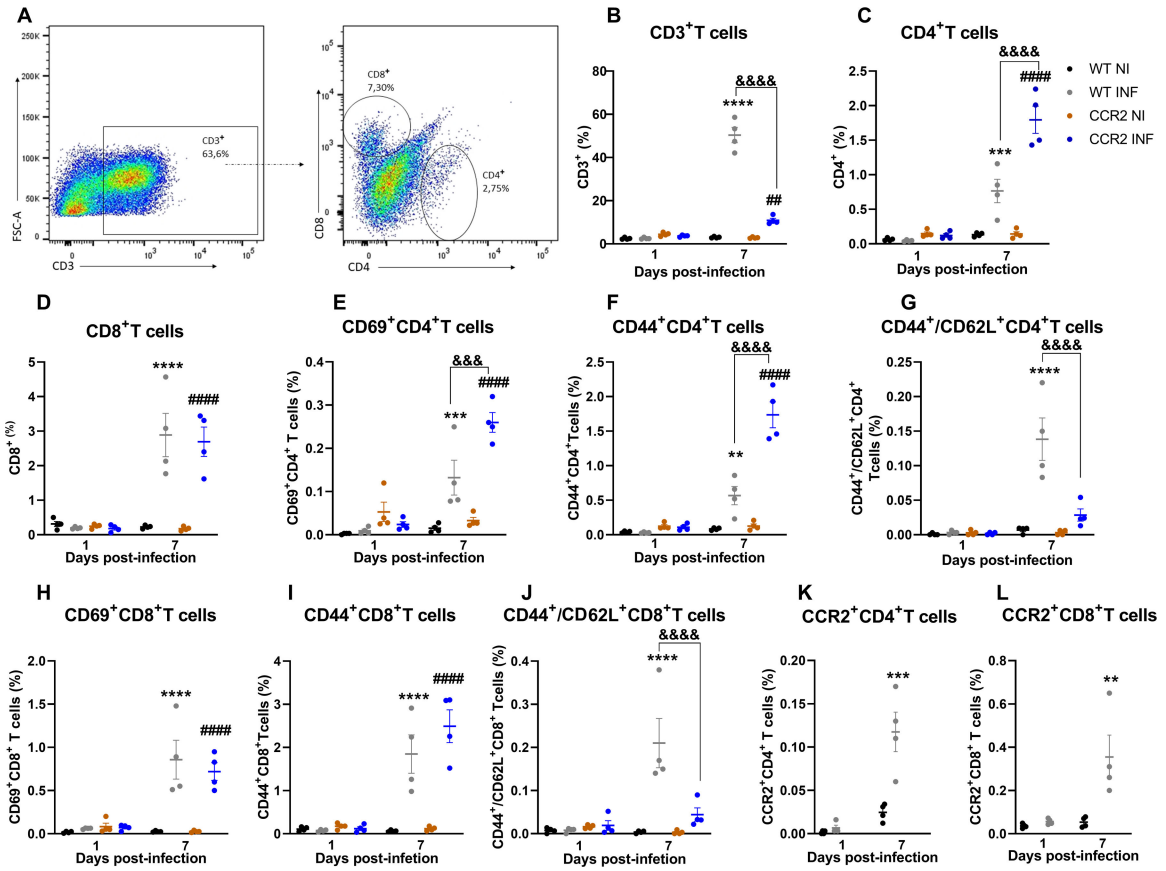


**FIG 7** Profile of lymphoid immune cells in the paw of MAYV-infected WT and $CCR2^{-/-}$ mice. Flow cytometry analysis of immune cells isolated from the hind paw of animals infected with MAYV at days 1 and 7 PI. (A) The panel shows the gating strategy for defining the population of lymphoid cells from the single cells. % of total cells were used to represent T cell subsets. (B) $CD3^+$ cell population. (C) $CD4^+$ T cell population. (D) $CD8^+$ T cell population. (E) Percentage of $CD4^+$ T cells expressing CD69. (F) Percentage of $CD4^+$ T cells expressing CD44. (G) Percentage of $CD4^+$ T cells expressing CD44/CD62L. (H) Percentage of $CD8^+$ T cells expressing CD69. (I) Percentage of $CD8^+$ T cells expressing CD44. (J) Percentage of $CD4^+$ T cells expressing CD44/CD62L. Percentage of $CD4^+$ T (K) and $CD8^+$ T (L) cells expressing $CCR^{-/-}$. Statistics were performed with two-way ANOVA, followed by Tukey's multiple comparisons test ($^*P$-value ≤0.05; $^{**}P$-value <0.01; $^{***}P$-value <0.001; $^{****}P$-value <0.0001). $^*$Difference between WT NI and WT INF; $^\#$difference between $CCR2^{-/-}$ NI and $CCR2^{-/-}$ INF; $^\&$difference between WT and $CCR2^{-/-}$. Data are derived from at least four mice per group (mean ± SEM).

hypernociception, bone loss, and viral load. Furthermore, the absence of monocytes at the site of infection may be associated with a delay in the onset of edema and recovery from tissue damage.

## Interference in the CCL2–CCR2 axis with two therapeutic approaches showed positive effects on important parameters of MAYV disease

In complementary experiments, we performed CCL2 gene silencing and pharmacological antagonism of the CCR2 receptor *in vivo* to understand the full role of the CCR2–CCL2 axis in the pathogenesis of MAYV and explore the therapeutic potential of these molecules. For the silencing, siRNA-CCL2 complexes of polymeric-lipid nanoparticle (NP-siRNA-CCL2) were used to silence the *ccl2* chemokine expression to support our findings in the CCL2/CCR2 pathway (Fig. 8A). We employed the dynamic light scattering (DLS) technique to determine the precise particle size, zeta potential, and polydispersity index (PDI). DLS measurements showed that the mean diameter of NP-siRNA-CCL2 was 121.3 nm (SD 0.55 nm), PDI 0.15 (SD 0.01), and zeta potential around −0.51 mV (SD 0.18 mV). Silencing *Ccl2* chemokine expression in WT mice with siRNA did not induce any effect on paw edema, although it improved the hypernociception thresholds significantly (Fig. 8B and C). Additionally, treatment of WT mice with SiCCL2 also decreased CCL2 levels and *Ccl2*, *Ccl*5, *Ccl7,* and *Tnf* expression in the hind paw tissue (Fig. 8D through I). However, silencing did not reduce the inflammatory infiltrate and histological damage (Fig. 8J and K; Table 1).

Additionally, we performed the pharmacological blockade of CCR2 with a CCR2 small antagonist molecule, RS504393. Interestingly, the treatment prevented the development of edema in infected mice and also promoted a significant improvement in the hypernociception threshold (Fig. 9A and B). However, the treatment had no effect on the viral load in most of the analyzed tissues, showing a discrete reduction only in the paw (Fig. 9C and D). Also, the CCR2 antagonist did not interfere with the levels of CXCL1 or CCL2, although it reduced the CCL5 concentrations in the paw (Fig. 9E through G). The histopathological analysis revealed a reduction in the percentage of mice presenting intense tissue damage and leukocyte infiltration after the treatment (Fig. 9H and I, i–iv). In view of the potential of MAYV to induce bone loss and the signaling role of CCR2 during this pathological process, we also investigated whether treatment with RS504393 would protect mice against bone resorption. The µCT results showed that the pharmacological treatment induced a milder protective phenotype than that observed in $CCR2^{-/-}$ mice. The mean values for total bone volume, trabecular separation, porosity, and trabecular number had a discrete reduction in mice treated with the CCR2 antagonist, but there was no statistical difference when compared with the vehicle-treated mice (Fig. 9J through M).

## Response of macrophages, osteoclasts, and osteoblasts against MAYV

Bone homeostasis is the result of a balance between osteocyte signaling, osteoblastic bone formation, and osteoclastic bone resorption (22). To understand the mechanism by which MAYV caused bone loss *in vivo*, we investigated the susceptibility and response of macrophages, osteoclasts, and osteoblasts after MAYV infection *in vitro*. Infection of primary culture WT and $CCR2^{-/-}$ macrophages with MAYV at MOI of 1 showed that although there was no productive infection (Fig. 10A) or loss of viability (Fig. 10D), MAYV modulated the production of cytokines by these cells. Macrophage response to infection resulted in IL-6 production only by WT cells (Fig. 10B), while TNF was significantly detected in $CCR2^{-/-}$ cells at 72 h PI (Fig. 10C). Similarly, MAYV was unable to promote a productive infection in primary osteoclasts [receptor activator of nuclear factor kappa-B ligand (RANKL)-differentiated] (Fig. 10E) but momentarily reduced the viability of the $CCR2^{-/-}$ cells after 24 and 48 h of infection (Fig. 10H). MAYV infection also induced the production of IL-6 (Fig. 10F) and TNF (Fig. 10G), two important pro-osteoclastogenic mediators, in both WT and $CCR2^{-/-}$ osteoclast cultures. Nevertheless, IL-6 production was significantly lower in $CCR2^{-/-}$ osteoclasts when compared to WT cells (Fig. 10F). To

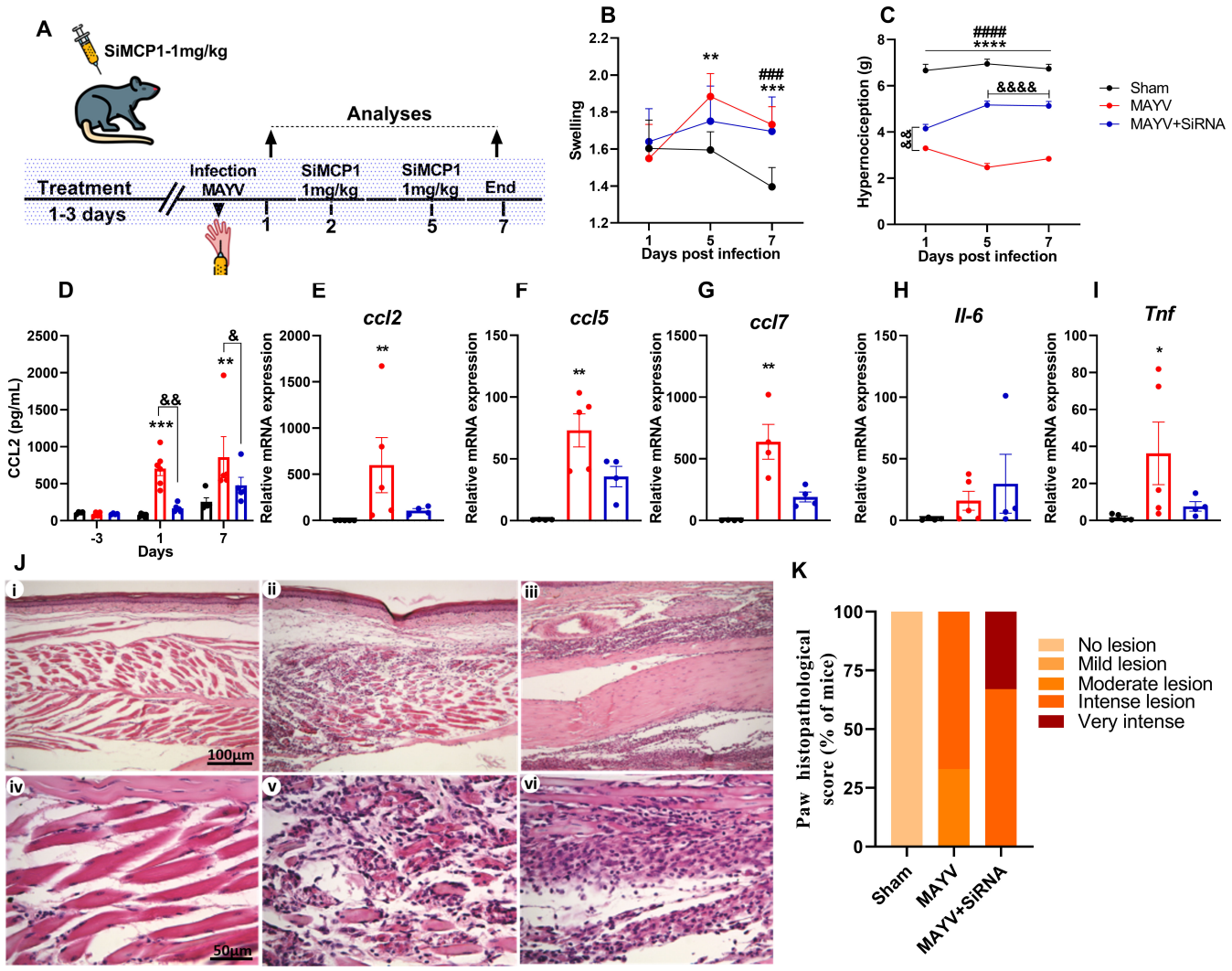


**FIG 8** CCL2 chemokine silencing in C57BL6 mice with siRNA. Four-week-old mice were treated for 3 days with NP-siRNA-CCL2 (NP-siRNA-MCP1) before infection and on days 2 and 5 post-infection. Animals were infected via the rear right footpad with $10^6$ PFU or mock-infected with PBS 1×. (A) Experimental design. (B) Edema measurements were performed in the infected paw (right paw) with the aid of a caliper on days 2 and 5 post-infection. (C) Hypernociception threshold assessment was performed using the von Frey method. Statistics were performed with two-way ANOVA, followed by Tukey's multiple comparisons test ($^{*}P$-value ≤0.05; $^{**}P$-value <0.01; $^{***}P$-value <0.001; $^{****}P$-value <0.0001). $^{*}$Difference between sham and MAYV; $^{\#}$difference between sham and MAYV+siRNA; $^{\&}$difference between MAYV and MAYV+siRNA. (D) Serum CCL2 levels on day −3 (before infection) and days 1 and 7 post-infection. (E–I) qRT-PCR analysis of the relative gene expression of the chemokines *Ccl2* (E), *Ccl5* (F), and *Ccl7* (G) and cytokines *Il-6* (H) and *Tnf* (I) in the paw. Statistics were performed with the Kruskal–Wallis test ($^{*}P$-value ≤0.05; $^{**}P$-value <0.01; $^{***}P$-value <0.001; $^{****}P$-value <0.0001). (J) Representative histological micrographs. At day 7 PI, mice were euthanized, ankle tissues were removed and paraffin-embedded, and 5 µm sections were generated and stained with H&E. The panel shows negative control (i and iv), animals infected with MAYV (ii and v), and animals infected and treated with SiMCP1 (iii and vi). (K) Histopathological paw score. Data are derived from at least four mice per group (mean ± SEM).

investigate the osteoblast response to infection, bone marrow-derived mesenchymal stem cells (BMSCs) were isolated and followed the differentiation protocol for 14 days. BMSCs isolated from WT and CCR2$^{-/-}$ animals were cultivated to compare the response of these cells *in vitro*. There was no productive MAYV infection in WT and CCR2$^{-/-}$ cells (Fig. 10I). Furthermore, no loss of viability (Fig. 10K) and changes in the alkaline phosphatase activity in osteoblasts with active CCR2 (NI: 0.224 ± 0.063 versus INF: 0.267 ± 0.091, $P$ = 0.9999) or CCR2$^{-/-}$ (NI: 0.219 ± 0.046 versus INF: 0.218 ± 0.057, $P$ > 0.9999) have been observed. Interestingly, IL-6 was produced exclusively by WT osteoblasts in response to MAYV infection (Fig. 10J), which suggests that the cytokine IL-6 plays an important role

**TABLE 1** Paw histopathological score from mice infected with MAYV and treated with siRNA-CCR2[a]

| Mice | Inflammatory infiltrate (0–4) | Muscle architecture loss (0–3) | Total | One-way ANOVA/Tukey's multiple comparisons test | Significant? | Adjusted *P*-value |
|---|---|---|---|---|---|---|
| Sham 1 | 0 | 0 | 0 | Sham vs MAYV | Yes | 0.0003 |
| Sham 2 | 0 | 0 | 0 | | *** | |
| Sham 3 | 0 | 0 | 0 | | | |
| MAYV 1 | 3 | 2 | 5 | Sham vs MAYV+siRNA | Yes | <0.0001 |
| MAYV 2 | 3 | 2 | 5 | | *** | |
| MAYV 3 | 2 | 2 | 4 | | | |
| MAYV+siRNA 1 | 4 | 3 | 7 | MAYV vs MAYV+siRNA | No | 0.1089 |
| MAYV+siRNA 2 | 3 | 2 | 5 | | ns | |
| MAYV+siRNA 3 | 4 | 2 | 6 | | | |

[a]Average score of $n = 3$ mice/group. 0, absent; 1–2, mild; 3–4, moderate; 5–6, intense; 7, severe.

in the mechanism of bone loss induced by MAYV. Similar results were detected when CCR2 was antagonized by RS504393, in which osteoblasts with active CCR2 showed a significant production of IL-6 after infection (NI: 879.73 ± 198.27 pg/mL versus INF: 2,966.72 ± 435.27 pg/mL, $P < 0.0001$) when compared to cells with blocked CCR2 (NI: 1,132.73 ± 643.82 pg/mL; INF: 1,250.96 ± 628.95 pg/mL, $P = 0.9921$). In summary, these data show that the inflammatory response to MAYV infection differs in the presence or absence of CCR2, which is associated with a lower production of the cytokine IL-6 in all cells with non-functional CCR2.

## DISCUSSION

MAYV is an emerging alphavirus in the American continent that has great potential for urbanization and has recently become an important public health problem in Brazil (23). MAYV, like RRV and CHIKV, is responsible for causing a highly debilitating musculoskeletal inflammatory disease, which includes polyarthralgia/polyarthritis and myalgia. The disease induced by arthritogenic alphaviruses is classified as an immunopathology (7, 24). Immunopathology is being increasingly recognized in many human viral diseases, such as dengue, zika, influenza, and more recently COVID-19 (25–27). Therefore, the investigation of the immune response mechanisms that influence the pathogenesis of MAYV infection would allow to design better treatment strategies to limit inflammation and tissue damage driven by inflammation (7). The major findings of the present study can be summarized as follows: (i) infection of C57BL/6J mice induced an acute inflammatory disease, characterized by local edema, hypernociception, myositis, replication in target organs, production of several inflammatory mediators, and bone resorption; (ii) absence of CCR2 receptor has a partial protective effect on MAYV infection, showed by signs of milder and delayed disease manifestation, reduced viral loads in several organs, less tissue damage, and absence of bone loss; (iii) the inflammatory profile of cell infiltrates of WT mice is predominantly composed of macrophages, whereas in $CCR2^{-/-}$ animals, it has been replaced by neutrophils; (iv) MAYV has the potential to modulate the intrinsic ability of osteoblasts, osteoclasts, and macrophages to produce pro-inflammatory cytokines related to bone resorption (Fig. 11).

Molecular and cellular mechanisms associated with MAYV pathogenesis are poorly understood. From animal models and studies with patients, MAYV, CHIKV, and RRV have been shown to induce a strong local pro-inflammatory response, characterized by the predominance of macrophages and pro-inflammatory mediators such as IL-6, TNF, INF-γ, and CCL2 (8, 13, 16, 28, 29). The CCL2–CCR2 axis has been proposed to be the main route responsible for the recruitment of monocytes and macrophages during alphaviral infections. Thus, studies on the role of monocytes/macrophages and CCL2–CCR2 axis in the infection by different arthritogenic alphaviruses would allow us to understand the interaction of alphaviruses with these factors and thus elucidate the mechanisms associated with the development of more severe disease (7).

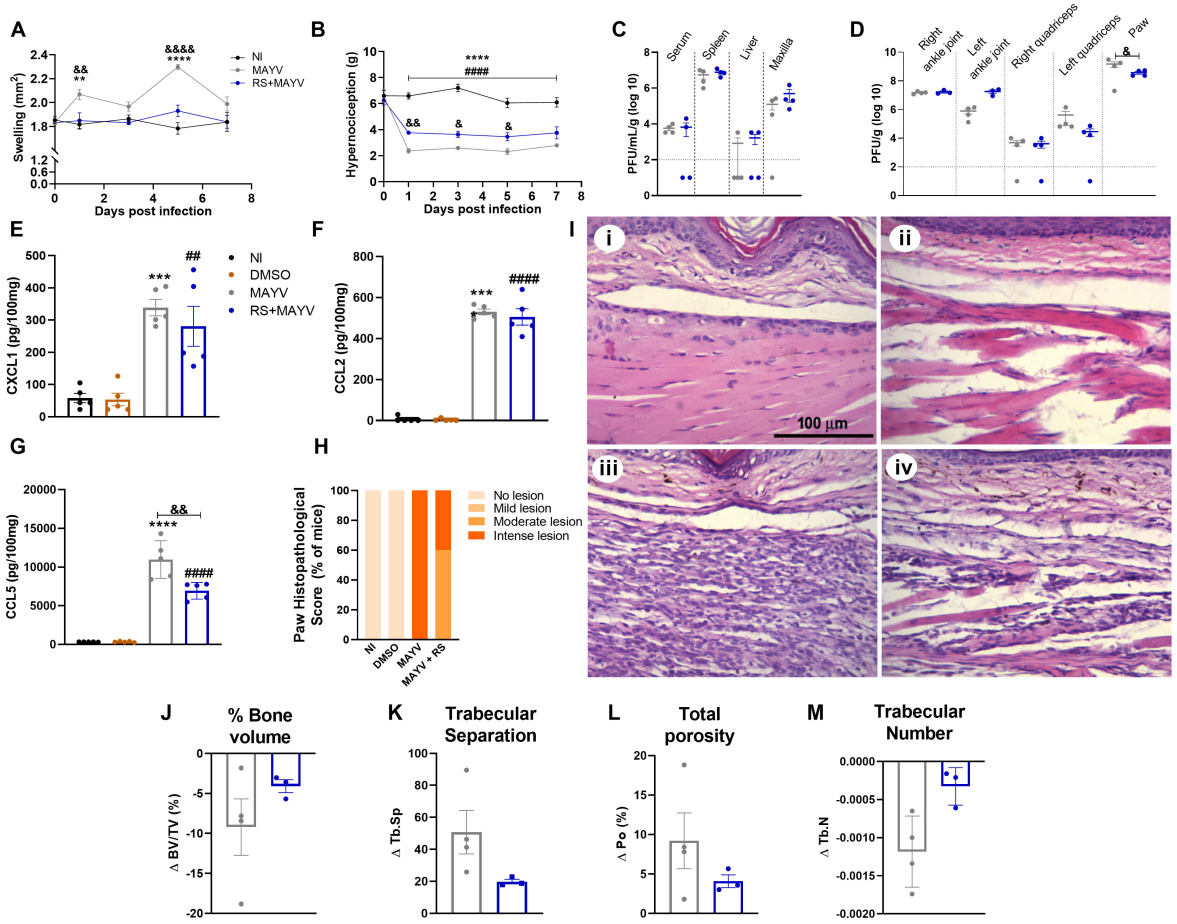


**FIG 9** Effect of CCR2 antagonism on MAYV-induced disease. Four-week-old mice were treated with RS504393 1 day before infection and every 24 h after infection until the point of analysis. To evaluate the edema and hypernociception, the animals were treated for 7 days with RS504393, and measurements were taken on days 0, 1, 3, 5, and 7 PI (A and B). Statistics were performed with two-way ANOVA and Tukey's multiple comparisons test ($^{*}P$-value ≤0.05; $^{**}P$-value <0.01; $^{***}P$-value <0.001; $^{****}P$-value <0.0001). $^{*}$Difference between MAYV and NI; $^{\#}$difference between RS+MAYV and NI; $^{\&}$difference between MAYV and RS+MAYV. To analyze the effect of RS504393 on viral load, the animals were treated up to day 2 PI, and the tissues were collected on day 3 PI (C and D). To evaluate the chemokine profile and the inflammatory process in the paw, the animals were treated until day 6 PI, and the paw tissues of interest were collected on day 7 PI. (E) CXCL1, (F) CCL3, and (G) CCL5 levels were evaluated by ELISA. Statistics were performed with one-way ANOVA, followed by Tukey's multiple comparisons test ($^{*}P$-value ≤0.05; $^{**}P$-value <0.01; $^{***}P$-value <0.001; $^{****}P$-value <0.0001). (H) Histopathological paw score. (I) Representative images of paw tissue samples. At day 7 PI, mice were euthanized, and paw tissues were removed and paraffin-embedded, and 5 µm sections were generated and stained with H&E. The panel shows negative control (i), group DMSO (ii), group infected with MAYV (iii), and group infected and treated with RS504393 (iv). With 20 days of treatment and 21 days PI, the mice were euthanized, and the tibia was collected for analysis by µCT. (J) % bone volume [BV/TV (%)], (K) trabecular separation (Tb.Sp), (L) total porosity [Po (%)], and (M) trabecular number (Tb.N). Statistics were performed with Student's unpaired *t*-test (no significant difference has been detected). Data are derived from at least four mice per group (mean ± SEM).

Our results show that infection of 4-week-old WT mice was characterized by MAYV replication and dissemination to various tissues, as well as induction of clinical disease signs, such as plantar edema and persistent articular hypernociception. These signs were accompanied by extensive inflammation of muscle tissue. These results are similar to those found in other animal models proposed for MAYV and other alphaviruses (13, 28, 30–32). The inflammatory response was characterized by the local production of the chemokines CCL2 and CCL5 and the cytokines IL-6 and TNF. Interestingly, we observed high levels of CCL2 systemically, in tissues such as the maxillae, muscle, paw, and spleen. Elevated levels of the CCL5 chemokine have also been detected in the quadriceps muscle. These inflammatory mediators have been reported in other animal models for MAYV, as well as CHIKV and RRV (8, 13, 28, 31, 33). Accordingly, patients with persistent

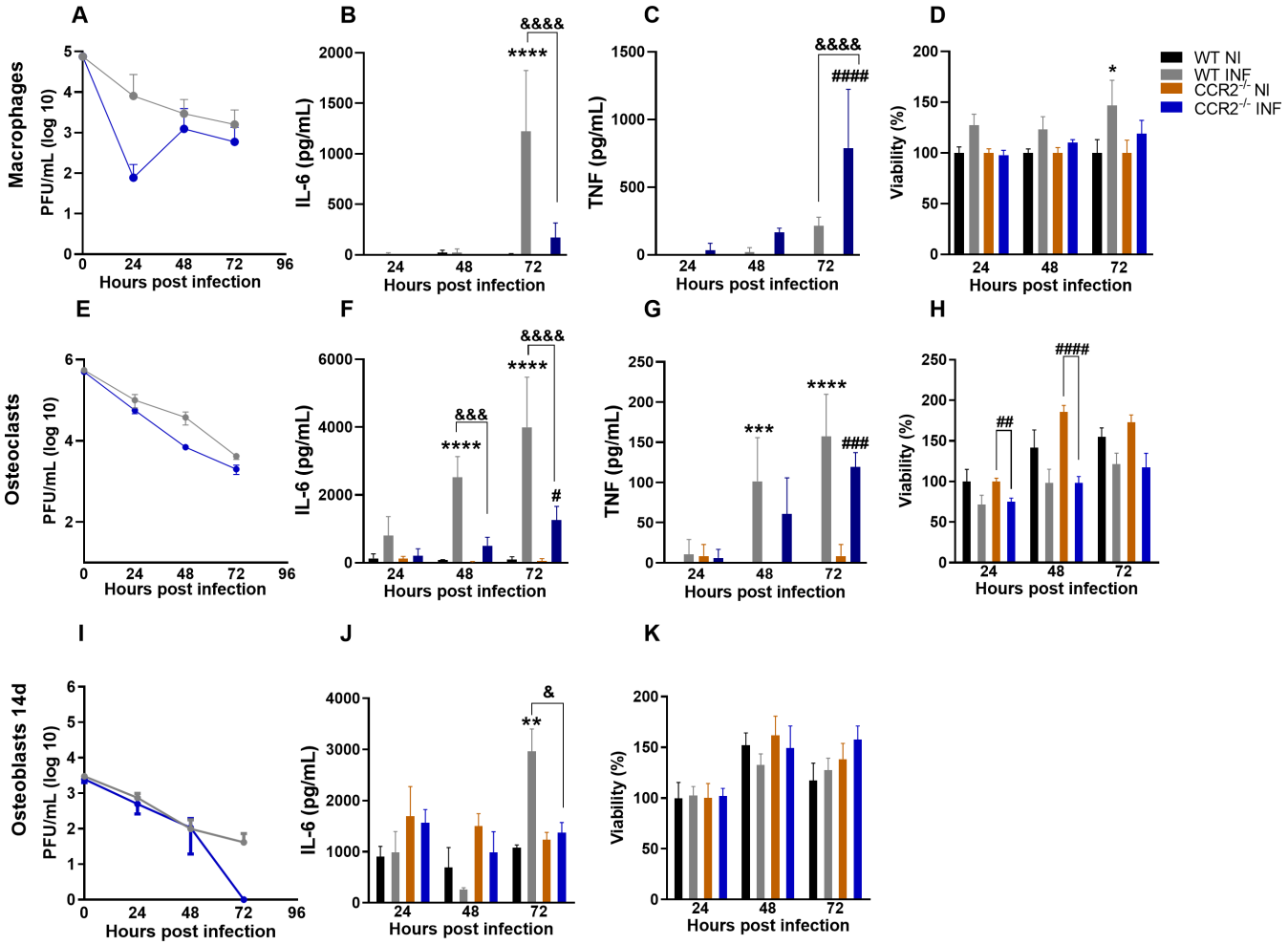


**FIG 10** *In vitro* infection of macrophages, osteoclast, and osteoblasts by MAYV. (A) MAYV titration in primary macrophages. (B) Quantification of IL-6 and (C) TNF levels in the macrophage culture supernatant. (D) Cell viability of primary culture of WT and CCR2$^{-/-}$ macrophages. (E) MAYV titration in primary osteoclasts. (F) Quantification of IL-6 and (G) TNF levels in the osteoclast culture supernatant. (H) Cell viability of primary culture of WT and CCR2$^{-/-}$ osteoclasts. (I) MAYV titration in the primary culture of osteoblasts from WT and CCR2$^{-/-}$ cells differentiated for 14 days. (J) Quantification of IL-6 in the osteoblast culture. (K) Cell viability of primary osteoblast culture of WT and CCR2$^{-/-}$ cells. Statistics were performed with two-way ANOVA, followed by Tukey's multiple comparisons test ($^{*}P$-value ≤0.05; $^{**}P$-value <0.01; $^{***}P$-value <0.001; $^{****}P$-value <0.0001). $^{*}$Difference between WT NI and WT INF; $^{\#}$difference between CCR2$^{-/-}$ NI and CCR2$^{-/-}$ INF; $^{\&}$difference between WT and CCR2$^{-/-}$. Data are derived from at least three biological replicates (mean ± SEM).

arthralgia during MAYV infection showed elevated levels of various inflammatory mediators, including the cytokine IL-6, which remained elevated for more than 12 months post-infection. The acute phase of the disease in these patients was marked by a high expression of CCL2 and remained elevated for months after infection (16). These mediators, which have been constantly reported in the serum of patients infected with different arthritogenic alphaviruses, indicate a common signature of the inflammatory response during infection with these viruses (6, 14, 16). Nevertheless, the role of each of these mediators in the pathogenesis of alphaviral diseases is not well established. CCL2 chemokine is important for the recruitment of monocytes/macrophages to the infection site, which are important cells in the development of myositis and arthritis (9, 10, 30). The cytokines IL-6 and TNF have been described as having an important role in tissue damage (31). In addition, CCL2 and the cytokine IL-6 have been associated with bone pathologies induced by CHIKV and RRV (11, 12, 34).

In inflammatory rheumatic diseases, inflammation is considered the main mechanism responsible for bone loss, and these cytokines have already been described as having a

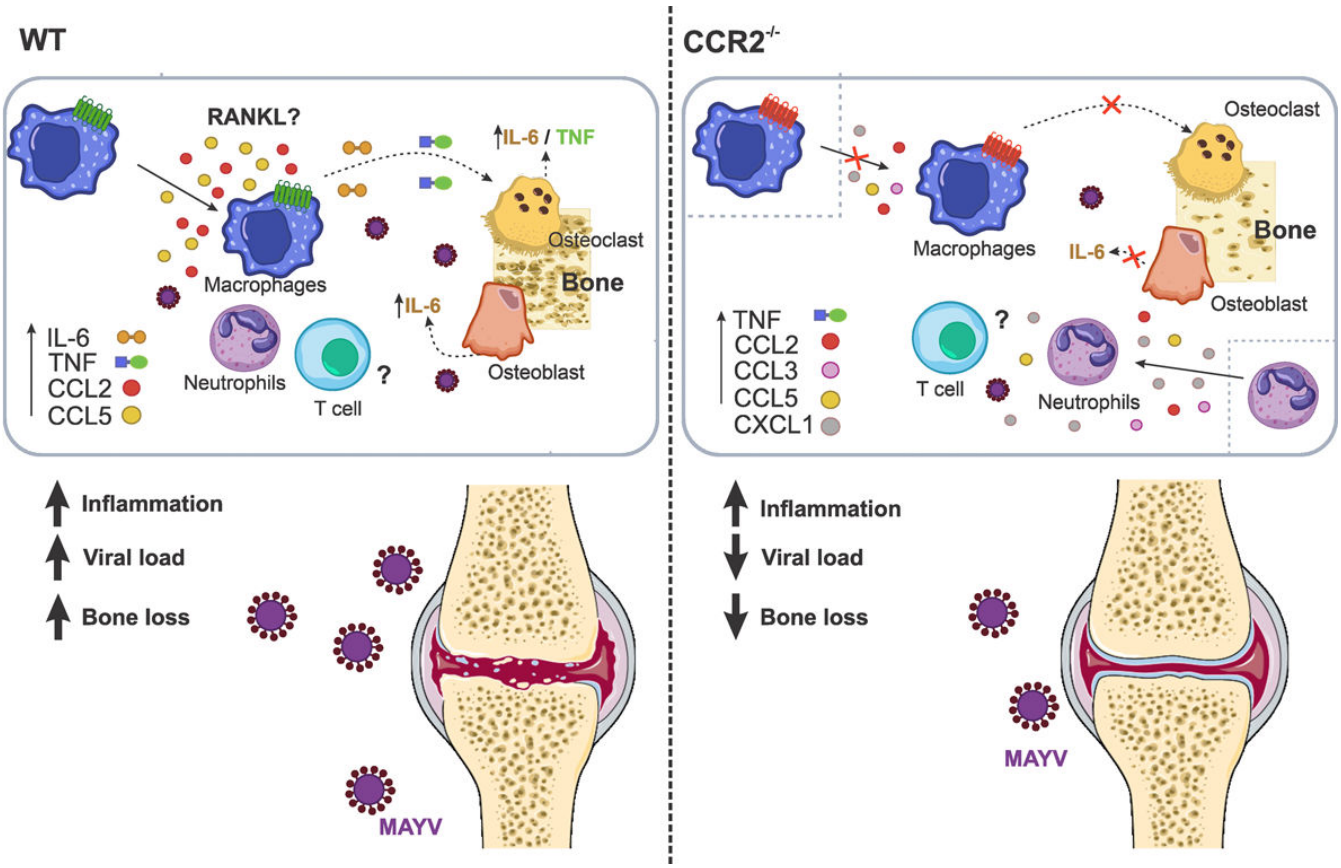


**FIG 11** Mechanism involved in osteoclastogenesis induced by MAYV. MAYV infection induces a robust inflammatory response at the infection site in WT and CCR2$^{-/-}$ animals, mediated by different pro-inflammatory cytokines and chemokines. This inflammatory process is responsible for tissue damage and also bone loss. The absence of bone loss in CCR2$^{-/-}$ animals showed that CCR2/CCL2 signaling is essential for the migration of macrophages to the infection site. The inflammatory microenvironment induced by MAYV in different cells promoted the differentiation of macrophages in osteoclasts by a mechanism probably independent on RANKL. It is suggested that the direct action of the cytokines IL-6 and TNF is able to support the formation of new osteoclasts. The increase in osteoclasts and their activity promotes bone loss. The role of T cells in bone loss from MAYV has not been investigated in this work.

central role in bone loss in RA and infection with other alphaviruses (11, 12, 22). The occurrence of bone erosion, similar to that of RA, has been reported in the joints of patients infected with CHIKV. Some studies in animal models for CHIKV and RRV, as well as in osteoblast cell culture, demonstrated that the inflammation induced in the bone microenvironment triggers osteoclast-mediated bone resorption (11, 12, 34). Chen et al. (11) showed that RRV infects osteoblasts and induces IL-6 production, which in turn leads to the increased expression of CCL2, changes in the RANKL:osteoprotegerin ratio, and consequently bone loss. The blockade of IL-6 and CCL2 in animal models for RRV and CHIKV was accompanied by a significant improvement in bone loss (9–12). In this work, we demonstrated that MAYV also has the potential to induce local bone loss. Thus, as observed for RRV and CHIKV, CCL2 appears to be a key mediator in MAYV-induced osteoclastogenesis, given its significant systemic increase in infected animals.

Arthritic disease is generally characterized by high levels of CCL2 and monocyte/macrophage infiltrates and is also well described for alphaviral arthropathies. Given the important role of this CCL2/CCR2 pathway in the pathology of many diseases, many therapeutic agents targeting the chemokine CCL2 and the CCR2 receptor have been developed (21). Treatment of mice infected with RRV or CHIKV with bindarit, a drug that inhibits the production of CCL2, resulted in the improvement of rheumatic disease induced by these viruses (9, 10, 12). However, the absence of CCR2 has been controversial in different rheumatic diseases (20, 35). Infection of CCR2$^{-/-}$ mice with CHIKV showed a more severe, prolonged, and erosive disease that was dominated by neutrophils,

with viral replication and persistence not being significantly affected (21). Interestingly, we demonstrated that CCR2$^{-/-}$ mice infected by MAYV had a milder and delayed disease manifestation, with reduced viral loads in some tissues, fast recovery of articular hypernociception, and absence of bone loss, when compared to WT. Paw edema and the peak of the inflammatory process in CCR2$^{-/-}$ mice were delayed in relation to the WT animals. This delay can be explained by the scarcity of M2 macrophages (CCR2$^{+}$ monocyte derivative) at the infection site, which are important cells for the resolution of inflammation and tissue regeneration. Poo et al. (21) demonstrated in their model of CCR2$^{-/-}$ mice for CHIKV a lower upregulation of M2 macrophage markers. Interestingly, as described for CHIKV, we observed a significant increase in CXCL-1 levels, accompanied by the replacement of an infiltrate of macrophages by neutrophils in the paw of CCR2$^{-/-}$ mice. The intense migration of CCR2$^{+}$ monocytes to the infection sites in WT animals suggests that these cells play a central role in MAYV-mediated bone loss in these animals. Accordingly, this data is strongly confirmed by the absence of bone loss observed in knockout mice, where there is an intense reduction in the influx of monocytes. In addition to this change in the cell migration profile, the absence of bone loss observed in knockout mice may also be associated with lower viral replication in target tissues and a reduced initial inflammatory response. In general, our data support a dual role for CCR2$^{+}$ monocytes/macrophages during MAYV infection, as they seem to be important for both the development of tissue damage and the resolution of the inflammatory process.

The lower viral replication observed in CCR2$^{-/-}$ mice may be associated with the relevant neutrophil infiltration in these animals during MAYV infection, suggesting that these cells are playing an important role in eliminating MAYV, without causing greater tissue damage. Recently, Hiroki et al. (36) reported that CHIKV induces the production of NETs in murine and human neutrophils *in vitro*, and the mechanism of induction of NETs in murine neutrophils by CHIKV is mediated by TRL7 and the production of ROS. Furthermore, it has been demonstrated both *in vitro* and *in vivo* that NETs have antiviral activity, promoting CHIKV neutralization and viral load control (36). Therefore, it would be interesting to investigate the role of neutrophils in controlling MAYV viral load, especially in CCR2$^{-/-}$ animals, and whether this control is related to the production of NETs. On the other hand, when we performed CCR2 blockade *in vivo*, we observed a difference in replication only in the paw, and no differences were detected in the *in vitro* experiments.

Silencing data showed that the reduction in CCL2 levels was associated with a partial improvement of clinical parameters, reinforcing the role of this pathway in the pathogenesis of MAYV. Furthermore, CCL2 silencing was also accompanied by a reduction in CCL5, CCL7, and TNF expression levels. This indicates that in the inflammatory microenvironment of MAYV infection, CCL2 secretion upregulates TNF expression, and TNF in turn stimulates the expression of CCL2 and CCL5 (37). This can result in a positive feedback loop between CCL2 and TNF. Nanki et al. (38) demonstrated that TNF regulated the production of CCL2 and CCL5 in fibroblast-like synoviocytes from patients with RA (17, 38, 39). In addition, our data also showed that CCL2 silencing modulates the expression of CCL7, an important chemokine that regulates monocytosis via CCR2 and that is often co-induced with CCL2 (37, 40). However, treatment was not enough to improve tissue damage induced by MAYV and reduce the inflammatory infiltrate, suggesting that probably other CCR2 ligands (CCL8, CCL13, and CCL12) or other inflammatory mediators in a CCR2-independent manner can induce the migration/accumulation of cells in the target tissue (41, 42). Drevets et al. (43) demonstrated that IFN-γ is essential for the influx of monocytes to the brain during systemic infection with virulent *Listeria monocytogenes* and was largely independent of a specific chemokine:receptor axis. Furthermore, the infection promoted an increase in the production of several chemokines involved in the recruitment of myeloid cells, and this explains the normal influxes of Ly6C$^{high}$ monocytes in the brain in mice deficient for CCL2, CCR1, CCR5, CXCR3, or CX3CR1 (43). This shows the importance of investigating CCR2-independent myeloid cell migration pathways in the pathogenesis of MAYV and other arthritogenic alphaviruses. Interestingly, these

data also show that hypernociception induced by MAYV infection is associated with the production of CCL2 and inflammatory cytokines such as TNF (44, 45). Accordingly, Kwiatkowski and colleagues (45) showed that the CCL2 chemokine plays a crucial role in the development of neuropathic pain in mice (45). In addition, the effect of pharmacological blockade of CCR2 on hypernociception induced by MAYV infection reveals that the CCR2–CCL2 pathway is a potential target for the clinical management of MAYV-induced pain.

However, the long and sustained blockade of CCR2 used in this work as a strategy to prevent tissue damage and bone loss did not present a significant protective effect. This result is similar to that found by Longobardi et al. in a model of OA, where they observed that long-term inhibition of 1–8 or 1–12 weeks did not prevent cartilage and bone damage, when compared with short-term treatment of 4 weeks. These findings suggest that prolonged CCR2 blockade may be ineffective in protecting against MAYV-induced joint damage and open new perspectives to explore different treatment strategies targeting CCR2 as a target molecule in MAYV-induced joint disease (46).

It has recently been shown that MAYV is capable of replicating in human osteoblasts, as well as in human chondrocytes and fibroblast-like synoviocytes (47). Many studies have also shown that CHIKV and RRV also replicate in cells that are important for arthritis induced by these viruses (11, 34, 48). In primary culture of WT and CCR2$^{-/-}$ osteoclasts, we observed that MAYV in MOI of 1 was not able to establish a productive infection in these cells but induced a high production of IL-6 and TNF mainly in WT cells. TNF and IL-6 are considered the most potent osteoclastogenic cytokines and play a central role in the pathogenesis of RA (49). These cytokines can stimulate osteoclastogenesis in two ways, by a mechanism independent of RANKL or indirectly by increasing the expression of RANKL and RANK, in osteoblasts and osteoclast precursors, respectively (50). Thus, according to *in vivo* and cell culture data, we suggest that the bone loss observed in WT animals may be caused by the direct action of TNF or IL-6, which is capable of inducing osteoclast formation and local osteolysis. The infection of WT and CCR2$^{-/-}$ macrophages resulted in the production of IL-6 and TNF, respectively. The infection of BMSCs isolated from 14 d.p.d. WT and CCR2$^{-/-}$ animals and WT osteoblasts with pharmacologically blocked CCR2 demonstrated that MAYV infection did not affect the osteogenic activity of these cells, unlike what was observed by Roy et al. (51), in that CHIKV reduced alkaline phosphatase activity in 9 d.p.d. infected osteoblasts. IL-6 production was induced by MAYV in WT osteoblasts. However, in pharmacologically blocked CCR2 or CCR2$^{-/-}$ cells, there was no production of IL-6. Taken together, these data show the importance of IL-6 production by osteoblasts in the bone microenvironment to promote the deregulation of homeostasis in bone tissue, as a consequence of MAYV infection.

Overall, our results demonstrate that the absence of CCL2/CCR2 signaling minimized the disease induced by MAYV and mitigated MAYV-driven bone loss. In this way, we were able to demonstrate one of the mechanisms underlying MAYV-induced bone pathology and consequently the role played by the CCL2/CCR2 axis as a potent therapeutic target.

## MATERIALS AND METHODS

### Cells, virus, and titration

Mayaro virus strain is a human isolate from Peru (in 2001) obtained from the World Reference Center for Emerging Viruses and Arboviruses at the University of Texas Medical Branch. MAYV stocks were produced on Vero cells CCL-81 from BCRJ (African green monkey kidney cell line). Briefly, Vero cells were grown in Dulbecco's modified Eagle's medium (DMEM) (Cultilab, Brazil) supplemented with 10% inactivated fetal bovine serum (FBS; Cultilab, Brazil) and 1% penicillin/streptomycin/glutamine (GIBCO) and kept in a humidified incubator at 37°C with 5% $CO_2$ atmosphere for 4 days. Cell supernatant was collected, centrifuged (2,000 rpm for 10 min), and then concentrated using a Vivacell 100 centrifugal concentrator (Sartorius). For MAYV titration, Vero cells were plated in 24-well

plates and infected with 10-fold serial dilutions. Plates were incubated for 72 h (37°C with 5% $CO_2$ atmosphere) and then fixed with 10% formaldehyde and stained with 1% violet crystal. Plaques were counted by eye.

### Infection of animals

Four-week-old male C57BL/6J mice (WT) were obtained from the Biotério Central of the Universidade Federal de Minas Gerais (UFMG). CCR2 receptor-deficient male mice ($CCR2^{-/-}$, genetic background C57BL/6J) were obtained from the Biotério de Imunofarmacologia of UFMG. WT and $CCR2^{-/-}$ mice were infected on the right footpad with $1 \times 10^6$ PFU of MAYV, with a final volume of 30 µL. Mock-infected mice received 30 µL of PBS 1×.

### Evaluation of disease parameters

Mice were observed up to 21 days after infection. During this period, every 24 h, mice were evaluated for signs of disease, such as weight loss, piloerection, and paw edema. Paw edema was quantified with the aid of a caliper, and measurements were performed on the infected paw, at time points 0, 1, 3, 5, 7, 10, 14, and 21 days after infection.

### Hypernociception assessment by a modified electronic pressure meter test von Frey method

Hypernociception was assessed as described by references (52). Briefly, mice were placed in acrylic boxes with a non-malleable wire floor for 15 minutes for acclimatization. Then, with the aid of a pressure transducer adapted to a standard large (0.5 $mm^2$) polypropylene tip (INSIGHT Instruments, Ribeirao Preto, SP, Brazil), an increasing pressure was exerted on the right hind paw of MOCK or MAYV-infected mice until the induction of the flexion of the knee joint, followed by paw withdrawal. Upon the flexion-elicited withdrawal threshold, the intensity of the pressure was automatically recorded. Two measurements were performed per animal at each time analyzed, and the median was used. Baseline measurements of all groups were initially performed before infection, and the remaining measurements were taken 1, 3, 7, 14, 21, and 28 days post-infection.

### ELISA assay

To assess the profile of cytokines and chemokines during infection, plasma and tissues of interest were collected at different post-infection times and assessed by ELISA using commercially available antibodies and according to the procedures supplied by the manufacturer (R&D Systems, Minneapolis). All samples were stored at −20°C until processing. Tissues were macerated in cytokine buffer and centrifuged at 10,000 rpm for 10 min at 4°C. The supernatant was collected and stored until the ELISA was performed. Results are expressed as pg/mL or pg/100 mg of tissue. The detection limit of the ELISA assays was in the range of 4–8 pg/mL.

### Micro-CT analysis

After euthanasia, the mouse right hind paw was removed, fixed in 10% formaldehyde, and then transferred to 70% alcohol, where they were kept until analysis in the micro-CT. Samples were scanned on a compact desktop micro-CT scanner (SkyScan 1174, Bruker micro-CT, Belgium) operating at 50 kV of source voltage, 800 µA source current, 14.59 µm pixel size, and 0.5 mm Al filter. Samples were attached to a stage that rotated 180° with images acquired every 0.7°. The acquired shadow projections (16-bit TIFF format) were further reconstructed into 2D slices using the NRecon software interface. 3D analyses were performed on the SkyScan CTAn tool, and 3D models were observed in the SkyScan CTVol interface. The following parameters were assessed: percentage of bone volume to total volume (%BV/TV), number of bone trabeculae (Tb.N), percentage of tissue porosity (%Po), and trabecular separation (Tb.Sp). In order to mitigate the baseline variations observed in these parameters between WT and $CCR2^{-/-}$ mice, all these data

were expressed as deltas by subtracting the value obtained in each infected mouse from the respective mean value of the uninfected mouse group. Therefore, the closer the results are to zero, the closer the values obtained between infected and uninfected animals.

## Histopathological analysis

After euthanasia, tissues of interest were removed and fixed in 10% formaldehyde. For the analysis of ankle joints, samples were decalcified in 10% EDTA, pH 7.0. Then, tissues were embedded in paraffin, and sections of 5 µm were performed. Analysis of tissue damage and inflammatory infiltrate was performed on mouse footpad samples-stained H&E slides. The samples were evaluated by a blinded pathologist using a score on inflammatory infiltrate and damage to muscle architecture, in a scale varying from no lesion to mild, moderate, intense, and very intense lesion. The data are presented as the percentage of mice presenting each lesion degree in each experimental group with a contingency table. To assess osteoclastogenesis, selected slides from the ankle joint with 21 days PI were stained for TRAP (Sigma-Aldrich, Saint Louis, MO, USA) and counterstained with hematoxylin according to the manufacturer's instructions.

## Footpad cell isolation

Footpad and ankle joints from control and MAYV-infected mice were collected at 1 and 7 days post-infection. For the isolation of cells from the plantar pad and ankle, tissues were removed and placed in 1 mL of digestion medium containing collagenase VIII (1 mg/mL; Sigma-Aldrich) in complete DMEM medium. Tissues were kept for 1 h in the water bath at 37°C. Then, the digested tissues were deposited in a 40 µm cell strainer (BD Falcon) and were added 3 mL complete DMEM medium. Digested tissues were macerated against the cell strainer with a 3 mL syringe plunger, making circular movements to release the largest number of cells in the medium. Cells were then centrifuged at 1,200 rpm for 10 minutes at 4°C and resuspended in 1 mL of complete medium. Cell viability was assessed with Trypan Blue.

## Phenotyping of leukocytes

Cells from the paw were plated on a 96-well plate with a U-shaped bottom to perform staining. First, the plate was centrifuged at 2,000 rpm for 10 min at 4°C to remove the medium. Cells were resuspended in 20 µL of Fc-blocker (BD Biosciences) for 15 minutes. Staining was performed using fluorescently conjugated antibodies (BD Biosciences) anti-CD3, -CD4, -CD8, -CD69, -CD44, -CD62L, -CCR2, -CD11c, -F4/80, -CD11b, -Ly6G, -Ly6C, -MHCII, and -CD80, for 30 min. Then, 200 µL of 1% BSA was added, and the cells were centrifuged to remove antibody excess. Cells were resuspended in 200 µL of 1% BSA, data were acquired using BD FACS CANTO II, and analysis was performed using the FlowJo software.

## Reverse transcription and real-time PCR analysis

WT mice were infected, and after euthanasia, paws were removed and stored at −80°C until processing. For total RNA extraction, samples were first mashed in liquid nitrogen and followed by TRIzol extraction according to the manufacturer's instructions. Reverse transcription was performed with random primers and following the guidelines of the iScript cDNA Synthesis Kit (Bio-Rad). The real-time PCR reaction was performed as follows: 2 µL of RT product (50 ng concentration), 1 µL of each primer, 5 µL of SYBR Green (qPCR Master Mix, Bio-Rad), and 2 µL of water. The conditions for PCR were as follows: 95°C for 2 min, followed by 40 cycles of 95°C for 15 s, 60°C for 1 min, and 72°C for 20 s. The efficiency/slope obtained values of all investigated genes were close to the optimal values required for the 2(−delta Ct) analysis (53). Ct values were recorded for each gene, and the results regarding the genes of interest were normalized to the results obtained

**TABLE 2** Primer sequences

| Primer | Sequence |
|---|---|
| IL-6 | F5′-TGTTCTCTGGGAAATCGTGAA3′ |
| | R5′-AAGTGCATCATCGTTGTTCATACA3′ |
| TNF | F5′-CCCTCACACTCAGATCATCTTCT3′ |
| | R5′-GCTACGACGTGGGCTACAG3′ |
| CCL2 | F5′-TAAAAACCTGGATCGGAACCAAA3′ |
| | R5′-GCATTAGCTTCAGATTTACGGGT-3′ |
| CCL5 | F5′-CAAGTGCTCCAATCTTGCAGTC3′ |
| | R5′-TCCTCTGGGTTGGCACACAC3′ |
| CCL7 | F: 5′TGGGAAGCTGTTATCTTCAAHACA3′ |
| | R: 5′CTCGACCCACT CTGATGGG3′ |
| RPS18 | F: 5′-TAGCCTTTGCCATCACTGCC3′ |
| | R: 5′-CATGAGCATATCTCCGGCCC3′ |
| PPIA | F: 5′-CAAACACAAACGGTTCCCAG3′ |
| | R: 5′-TTCACCTTCCCAAAGACCAC3′ |

with the internal control genes, *RPS18 and PPIA*. The ΔΔCT values were calculated, and the results were expressed as fold increase, as described by Krohn-Grimberghe et al. (54). The sequences of primers are shown in Table 2.

## *In vivo* silencing of the CCL2 chemokine with siRNA

Nanoparticles carrying siRNA-MCP1 (NP-siRNA-CCL2) were synthesized according to Krohn-Grimberghe et al. (55). For the silencing of the CCL2 chemokine, 4-week-old animals of the C57BL/6J strain were divided into three experimental groups: (i) sham: received only PBS, (ii) MAYV: infected only, and (iii) MAYV+siRNA: infected and treated. The animals in the treated group received 1 mg/kg intravenously. The treatment strategy included a pre-treatment for 3 days, every 24 h, before infection and post-infection treatments on days 2 and 5. After infection, the animals were evaluated for disease parameters, such as edema and hypernociception at defined time points. On day 7 PI, the animals were sacrificed, and the tissues of interest were removed for the following analyses, viral load, histology, ELISA, and gene expression.

## *In vivo* CCR2 antagonism

For systemic CCR2 receptor blockade, mice were treated with RS504393 (Sigma-Aldrich), a CCR2 antagonist. Treatment started 24 h before infection with MAYV. Every 24 h until the end of the experiment, the mice received intraperitoneal injections of 2 mg/kg of RS504393 (dissolved in DMSO at 10 mM and diluted in PBS for application, groups RS504393 and MAYV+RS504393). Untreated groups (NI group) received 100 µL of sterile PBS or DMSO 10 mM in PBS (DMSO group).

## Cell culture

For primary osteoblast, osteoclast, and macrophage cultures, bone marrow cells derived from WT and $CCR2^{-/-}$ mice were isolated and kept in culture for growth, in α-MEM medium with 10% FBS at 37°C and 5% $CO_2$. For the osteoblast culture, the cells were then plated into 96- or 24-well plates, and differentiation was induced with an osteogenic medium [α-MEM medium 10% plus 100 µM ascorbic acid and 1.8 nM potassium phosphate ($KH_2PO_4$)] for 14 days. To evaluate the effect of blocking CCR2 in osteoblast culture, cells were treated 1 h before infection with the antagonist RS504393 (300 nM per well). Every 2 days, the medium was replaced with a new medium. After differentiation, cells were infected with MAYV, and the cell supernatant was collected at different time points post-infection. Several analyses were performed, including viral titration, ELISA, cell viability (MTT), and alkaline phosphatase labeling. For the macrophage culture,

the cells were then plated into a 96-well plate, and differentiation was induced with 50 ng/mL of M-CSF for 3 days. After differentiation, cells were infected with MAYV, and the cell supernatant was collected at different time points post-infection for analysis. For osteoclast culture, the cells were then plated into a 96-well plate, and differentiation was induced with 50 ng/mL of M-CSF (Peprotech Inc.) and 50 ng/mL of RANKL (Peprotech Inc.) for 5 days.

### Statistical analysis

All analyses were performed using GraphPad PRISM software 6.0 (GraphPad Software, USA). Results with $P < 0.05$ were considered significant. Differences were compared using one- or two-way ANOVA followed by Tukey's multiple comparisons test or unpaired *t*-test.

## ACKNOWLEDGMENTS

The authors would like to thank Ilma Marçal, Tania Colina, Frankcineia Assis, and Gilvania Santos for the technical support.

This work received financial support from the National Institute of Science and Technology in Dengue and Host–Microorganism Interaction (INCT dengue), a program funded by the Brazilian National Science Council (CNPq, Brazil process 465425/2014-3) and Minas Gerais Foundation for Science (FAPEMIG, Brazil process 25036/2014-3), and from Rede de Pesquisa em Imunobiológicos e Biofármacos para terapias avançadas e inovadoras (ImunoBioFar), provided by FAPEMIG under process RED-00202-22" 29568-1 and FAPEMIG process APQ-02281-18. This study was also financed in part by the Coordenação de Aperfeiçoamento de Pessoal de Nível Superior (CAPES, Brazil), process 88881.507175/2020-01. M.L.N. was funded by the Centers for Research on Emerging Infectious Diseases (CREID) "Coordinating Research on Emerging Arboviral Threats Encompassing the Neotropics (CREATE-NEO)" grant number 1U01AI151807. The authors thank L'Oréal-UNESCO-ABC "Para Mulheres na Ciência" prize granted to V.V.C. and the PhD scholarship provided by CAPES to F.M.S.

F.M.S. performed the conceptualization, data curation, formal analysis, investigation, methodology, visualization, and writing—original draft. V.R.C.M. performed the investigation and methodology. S.A. performed the data curation, investigation, and methodology. C.D.F.S. performed the data curation, investigation, and methodology. T.P.M. performed the data curation, investigation, and methodology. M.R.G. performed the investigation and methodology. B.R.B. performed the methodology. A.C.P.M.S. performed the methodology. H.A.S. performed the data curation, investigation, methodology, review, and editing. P.A.C.C. performed the data curation, investigation, methodology, review, and editing. B.R.B. performed the investigation and methodology. P.B.S. performed the RT-qPCR standardization, data curation, analysis of the results, and writing—review and editing. M.M.P. performed the methodology and secured the resources. M.L.N. and D.S.G. secured the resources. P.P.G.G. secured the resources and performed the investigation and writing—review and editing. M.M.T. performed the funding acquisition and secured the resources. C.M.Q.J. performed the data curation, investigation, supervision, visualization, and writing—review and editing. V.V.C. performed the funding acquisition, investigation, project administration, supervision, validation, visualization, and writing—review and editing.

## AUTHOR AFFILIATIONS

[1]Department of Morphology, Drug Research and Development Center, Federal University of Minas Gerais, Belo Horizonte, Minas Gerais, Brazil
[2]Department of Physiology and Biophysics, Federal University of Minas Gerais, Belo Horizonte, Minas Gerais, Brazil
[3]Department of Microbiology, Host Microorganism Interaction Laboratory, Federal University of Minas Gerais, Belo Horizonte, Minas Gerais, Brazil

[4]Department of Metallurgical and Materials Engineering, Federal University of Minas Gerais, Belo Horizonte, Minas Gerais, Brazil
[5]Virology Research Laboratory, São José do Rio Preto School of Medicine (FAMERP), São José do Rio Preto, São Paulo, Brazil
[6]Department of Biochemistry and Immunology, Drug Research and Development Center, Federal University of Minas Gerais, Belo Horizonte, Minas Gerais, Brazil

## AUTHOR ORCIDs

Franciele Martins Santos http://orcid.org/0000-0002-8768-610X
Paula Bargi-Souza http://orcid.org/0000-0001-7746-0636
Danielle da Glória Souza http://orcid.org/0000-0002-7478-5934
Celso Martins Queiroz-Junior http://orcid.org/0000-0002-7884-7709
Vivian Vasconcelos Costa http://orcid.org/0000-0002-0175-642X

## FUNDING

| Funder | Grant(s) | Author(s) |
|---|---|---|
| Conselho Nacional de Desenvolvimento Científico e Tecnológico (CNPq) | 465425/2014-3 | Mauro Martins Teixeira |
| Fundação de Amparo à Pesquisa do Estado de Minas Gerais (FAPEMIG) | RED-00202-22 | Mauro Martins Teixeira |
| Fundação de Amparo à Pesquisa do Estado de Minas Gerais (FAPEMIG) | 25036/2014-3 | Mauro Martins Teixeira |
| L'Oréal-UNESCO-ABC 'Para Mulheres na Ciência' | | Vivian Vasconcelos Costa |
| Fundação de Amparo à Pesquisa do Estado de Minas Gerais (FAPEMIG) | APQ-02281-18 | Vivian Vasconcelos Costa |
| International Society of Neurochemistry | 29344 | Vivian Vasconcelos Costa |
| Centers for Research on Emerging Infectious Diseases (CREID) | 1U01AI151807 | Maurício Lacerda Nogueira |

## AUTHOR CONTRIBUTIONS

Franciele Martins Santos, Conceptualization, Data curation, Formal analysis, Investigation, Methodology, Visualization, Writing – original draft, Writing – review and editing | Victor Rodrigues de Melo Costa, Investigation, Methodology | Simone de Araújo, Investigation, Methodology | Carla Daiane Ferreira de Sousa, Data curation, Investigation, Methodology | Thaiane Pinto Moreira, Data curation, Investigation, Methodology | Matheus Rodrigues Gonçalves, Investigation, Methodology | Anna Clara Paiva Menezes dos Santos, Methodology | Heloísa Athayde Seabra Ferreira, Investigation, Methodology, Writing – review and editing | Pedro Augusto Carvalho Costa, Investigation, Methodology, Writing – review and editing | Breno Rocha Barrioni, Investigation, Methodology | Paula Bargi-Souza, Data curation, Formal analysis, Writing – review and editing | Marivalda de Magalhães Pereira, Methodology, Resources | Maurício Lacerda Nogueira, Resources | Danielle da Glória Souza, Resources | Pedro Pires Goulart Guimarães, Investigation, Resources, Writing – review and editing | Mauro Martins Teixeira, Funding acquisition, Resources | Celso Martins Queiroz-Junior, Data curation, Investigation, Supervision, Visualization, Writing – review and editing | Vivian Vasconcelos Costa, Funding acquisition, Investigation, Project administration, Supervision, Validation, Visualization, Writing – review and editing

## ETHICAL APPROVAL

This study was carried out in strict accordance with the Brazilian Government's ethical and animal experiments regulations (Law 11794/2008). The experimental protocol was

approved by the Committee on the Ethics of Animal Experiments of the Universidade Federal de Minas Gerais (CEUA/UFMG, Protocol Number 160/2018). All surgeries were performed under ketamine/xylazine anesthesia, and all efforts were made to minimize animal suffering.

## REFERENCES


1. Acosta-Ampudia Y, Monsalve DM, Rodríguez Y, Pacheco Y, Anaya J-M, Ramírez-Santana C. 2018. Mayaro: an emerging viral threat?. Emerg Microbes Infect 7:163. https://doi.org/10.1038/s41426-018-0163-5
2. Mota M de O, Ribeiro MR, Vedovello D, Nogueira ML. 2015. Mayaro virus: a neglected arbovirus of the Americas. Future Virol 10:1109–1122. https://doi.org/10.2217/fvl.15.76
3. Halsey ES, Siles C, Guevara C, Vilcarromero S, Jhonston EJ, Ramal C, Aguilar PV, Ampuero JS. 2013. Mayaro virus infection, Amazon basin region, Peru, 2010–2013. Emerg Infect Dis 19:1839–1842. https://doi.org/10.3201/eid1911.130777
4. Theilacker C, Held J, Allering L, Emmerich P, Schmidt-Chanasit J, Kern WV, Panning M. 2013. Prolonged polyarthralgia in a German traveller with Mayaro virus infection without inflammatory correlates. BMC Infect Dis 13:369. https://doi.org/10.1186/1471-2334-13-369
5. Slegers CAD, Keuter M, Günther S, Schmidt-Chanasit J, van der Ven AJ, de Mast Q. 2014. Persisting arthralgia due to Mayaro virus infection in a traveler from Brazil: is there a risk for attendants to the 2014 FIFA World Cup? J Clin Virol 60:317–319. https://doi.org/10.1016/j.jcv.2014.04.020
6. Tappe D, Pérez-Girón JV, Just-Nübling G, Schuster G, Gómez-Medina S, Günther S, Muñoz-Fontela C, Schmidt-Chanasit J. 2016. Sustained elevated cytokine levels during recovery phase of Mayaro virus infection. Emerg Infect Dis 22:750–752. https://doi.org/10.3201/eid2204.151502
7. Mostafavi H, Abeyratne E, Zaid A, Taylor A. 2019. Arthritogenic alphavirus-induced immunopathology and targeting host inflammation as A therapeutic strategy for alphaviral disease. Viruses 11:290. https://doi.org/10.3390/v11030290
8. Lidbury BA, Rulli NE, Suhrbier A, Smith PN, McColl SR, Cunningham AL, Tarkowski A, van Rooijen N, Fraser RJ, Mahalingam S. 2008. Macrophage-derived proinflammatory factors contribute to the development of arthritis and myositis after infection with an arthrogenic alphavirus. J Infect Dis 197:1585–1593. https://doi.org/10.1086/587841
9. Rulli NE, Guglielmotti A, Mangano G, Rolph MS, Apicella C, Zaid A, Suhrbier A, Mahalingam S. 2009. Amelioration of alphavirus-induced arthritis and myositis in a mouse model by treatment with bindarit, an inhibitor of monocyte chemotactic proteins. Arthritis Rheum 60:2513–2523. https://doi.org/10.1002/art.24682
10. Rulli NE, Rolph MS, Srikiatkhachorn A, Anantapreecha S, Guglielmotti A, Mahalingam S. 2011. Protection from arthritis and myositis in a mouse model of acute Chikungunya virus disease by bindarit, an inhibitor of monocyte chemotactic protein-1 synthesis. J Infect Dis 204:1026–1030. https://doi.org/10.1093/infdis/jir470
11. Chen W, Foo S-S, Li RW, Smith PN, Mahalingam S. 2014. Osteoblasts from osteoarthritis patients show enhanced susceptibility to Ross River virus infection associated with delayed type I interferon responses. Virol J 11:189. https://doi.org/10.1186/s12985-014-0189-9
12. Chen W, Foo S-S, Sims NA, Herrero LJ, Walsh NC, Mahalingam S. 2015. Arthritogenic alphaviruses: new insights into arthritis and bone pathology. Trends Microbiol 23:35–43. https://doi.org/10.1016/j.tim.2014.09.005
13. Santos FM, Dias RS, de Oliveira MD, Costa I, Fernandes L de S, Pessoa CR, da Matta SLP, Costa VV, Souza DG, da Silva CC, de Paula SO. 2019. Animal model of arthritis and myositis induced by the Mayaro virus. PLoS Negl Trop Dis 13:e0007375. https://doi.org/10.1371/journal.pntd.0007375
14. Teng T-S, Kam Y-W, Lee B, Hapuarachchi HC, Wimal A, Ng L-C, Ng LFP. 2015. A systematic meta-analysis of immune signatures in patients with acute Chikungunya virus infection. J Infect Dis 211:1925–1935. https://doi.org/10.1093/infdis/jiv049
15. Haist KC, Burrack KS, Davenport BJ, Morrison TE. 2017. Inflammatory monocytes mediate control of acute alphavirus infection in mice. PLoS Pathog 13:e1006748. https://doi.org/10.1371/journal.ppat.1006748
16. Santiago FW, Halsey ES, Siles C, Vilcarromero S, Guevara C, Silvas JA, Ramal C, Ampuero JS, Aguilar PV. 2015. Long-term arthralgia after Mayaro virus infection correlates with sustained pro-inflammatory cytokine response. PLoS Negl Trop Dis 9:e0004104. https://doi.org/10.1371/journal.pntd.0004104
17. Gschwandtner M, Derler R, Midwood KS. 2019. More than just attractive: how CCL2 influences myeloid cell behavior beyond chemotaxis. Front Immunol 10:2759. https://doi.org/10.3389/fimmu.2019.02759
18. Miller RE, Tran PB, Das R, Ghoreishi-Haack N, Ren D, Miller RJ, Malfait A-M. 2012. CCR2 chemokine receptor signaling mediates pain in experimental osteoarthritis. Proc Natl Acad Sci U S A 109:20602–20607. https://doi.org/10.1073/pnas.1209294110
19. Chen C-Y, Fuh L-J, Huang C-C, Hsu C-J, Su C-M, Liu S-C, Lin Y-M, Tang C-H. 2017. Enhancement of CCL2 expression and monocyte migration by CCN1 in osteoblasts through inhibiting miR-518a-5p: implication of rheumatoid arthritis therapy. Sci Rep 7:421. https://doi.org/10.1038/s41598-017-00513-0
20. Raghu H, Lepus CM, Wang Q, Wong HH, Lingampalli N, Oliviero F, Punzi L, Giori NJ, Goodman SB, Chu CR, Sokolove JB, Robinson WH. 2017. CCL2/CCR2, but not CCL5/CCR5, mediates monocyte recruitment, inflammation and cartilage destruction in osteoarthritis. Ann Rheum Dis 76:914–922. https://doi.org/10.1136/annrheumdis-2016-210426
21. Poo YS, Nakaya H, Gardner J, Larcher T, Schroder WA, Le TT, Major LD, Suhrbier A. 2014. CCR2 deficiency promotes exacerbated chronic erosive neutrophil-dominated Chikungunya virus arthritis. J Virol 88:6862–6872. https://doi.org/10.1128/JVI.03364-13
22. Coury F, Peyruchaud O, Machuca-Gayet I. 2019. Osteoimmunology of bone loss in inflammatory rheumatic diseases. Front Immunol 10:679. https://doi.org/10.3389/fimmu.2019.00679
23. Hotez PJ, Murray KO, Gubler DJ. 2017. West nile virus, Chikungunya, Zika—and now Mayaro? PLoS Negl Trop Dis 11:e0005462. https://doi.org/10.1371/journal.pntd.0005462
24. Assunção-Miranda I, Cruz-Oliveira C, Da Poian AT. 2013. Molecular mechanisms involved in the pathogenesis of alphavirus-induced arthritis. Biomed Res Int 2013:973516. https://doi.org/10.1155/2013/973516
25. Damjanovic D, Small C-L, Jeyanathan M, McCormick S, Xing Z. 2012. Immunopathology in influenza virus infection: uncoupling the friend from foe. Clin Immunol 144:57–69. https://doi.org/10.1016/j.clim.2012.05.005
26. Culshaw A, Mongkolsapaya J, Screaton GR. 2017. The immunopathology of dengue and Zika virus infections. Curr Opin Immunol 48:1–6. https://doi.org/10.1016/j.coi.2017.07.001
27. Gustine JN, Jones D. 2021. Immunopathology of hyperinflammation in COVID-19. Am J Pathol 191:4–17. https://doi.org/10.1016/j.ajpath.2020.08.009
28. Gardner J, Anraku I, Le TT, Larcher T, Major L, Roques P, Schroder WA, Higgs S, Suhrbier A. 2010. Chikungunya virus arthritis in adult wild-type mice. J Virol 84:8021–8032. https://doi.org/10.1128/JVI.02603-09
29. Ng LFP. 2017. Immunopathology of Chikungunya virus infection: lessons learned from patients and animal models. Annu Rev Virol 4:413–427. https://doi.org/10.1146/annurev-virology-101416-041808
30. Morrison TE, Whitmore AC, Shabman RS, Lidbury BA, Mahalingam S, Heise MT. 2006. Characterization of Ross River virus tropism and virus-induced inflammation in a mouse model of viral arthritis and myositis. J Virol 80:737–749. https://doi.org/10.1128/JVI.80.2.737-749.2006
31. Figueiredo CM, Neris R da S, Gavino-Leopoldino D, da Silva MOL, Almeida JS, Dos-Santos JS, Figueiredo CP, Bellio M, Bozza MT, Assunção-Miranda I. 2019. Mayaro virus replication restriction and induction of muscular inflammation in mice are dependent on age, type-I interferon response, and adaptive immunity. Front Microbiol 10:2246. https://doi.org/10.3389/fmicb.2019.02246
32. Mota M de O, Costa VV, Sugimoto MA, Guimarães G de F, Queiroz-Junior CM, Moreira TP, de Sousa CD, Santos FM, Queiroz VF, Passos I, Hubner J, Souza DG, Weaver SC, Teixeira MM, Nogueira ML. 2020. In-depth

characterization of a novel live-attenuated Mayaro virus vaccine candidate using an immunocompetent mouse model of Mayaro disease. Sci Rep 10:5306. https://doi.org/10.1038/s41598-020-62084-x
33. Herrero LJ, Nelson M, Srikiatkhachorn A, Gu R, Anantapreecha S, Fingerle-Rowson G, Bucala R, Morand E, Santos LL, Mahalingam S. 2011. Critical role for macrophage migration inhibitory factor (MIF) in Ross River virus-induced arthritis and myositis. Proc Natl Acad Sci U S A 108:12048–12053. https://doi.org/10.1073/pnas.1101089108
34. Noret M, Herrero L, Rulli N, Rolph M, Smith PN, Li RW, Roques P, Gras G, Mahalingam S. 2012. Interleukin 6, RANKL, and osteoprotegerin expression by Chikungunya virus-infected human osteoblasts. J Infect Dis 206:455–457. https://doi.org/10.1093/infdis/jis368
35. Quinones MP, Estrada CA, Kalkonde Y, Ahuja SK, Kuziel WA, Mack M, Ahuja SS. 2005. The complex role of the chemokine receptor CCR2 in collagen-induced arthritis: implications for therapeutic targeting of CCR2 in rheumatoid arthritis. J Mol Med (Berl) 83:672–681. https://doi.org/10.1007/s00109-005-0637-5
36. Hiroki CH, Toller-Kawahisa JE, Fumagalli MJ, Colon DF, Figueiredo LTM, Fonseca B, Franca RFO, Cunha FQ. 2019. Neutrophil extracellular traps effectively control acute Chikungunya virus infection. Front Immunol 10:3108. https://doi.org/10.3389/fimmu.2019.03108
37. Proost P, Wuyts A, Van Damme J. 1996. Human monocyte chemotactic proteins-2 and -3: structural and functional comparison with MCP-1. J Leukoc Biol 59:67–74. https://doi.org/10.1002/jlb.59.1.67
38. Nanki T, Nagasaka K, Hayashida K, Saita Y, Miyasaka N. 2001. Chemokines regulate IL-6 and IL-8 production by fibroblast-like synoviocytes from patients with rheumatoid arthritis. J Immunol 167:5381–5385. https://doi.org/10.4049/jimmunol.167.9.5381
39. Neumark E, Sagi-Assif O, Shalmon B, Ben-Baruch A, Witz IP. 2003. Progression of mouse mammary tumors: MCP-1-TNF? cross-regulatory pathway and clonal expression of promalignancy and antimalignancy factors. Int J Cancer 106:879–886. https://doi.org/10.1002/ijc.11337
40. Bardina SV, Michlmayr D, Hoffman KW, Obara CJ, Sum J, Charo IF, Lu W, Pletnev AG, Lim JK. 2015. Differential roles of chemokines CCL2 and CCL7 in monocytosis and leukocyte migration during West Nile virus infection. J Immunol 195:4306–4318. https://doi.org/10.4049/jimmunol.1500352
41. Haringman JJ, Tak PP. 2004. Chemokine blockade: a new era in the treatment of rheumatoid arthritis? Arthritis Res Ther 6:93–97. https://doi.org/10.1186/ar1172
42. Shi C, Pamer EG. 2011. Monocyte recruitment during infection and inflammation. Nat Rev Immunol 11:762–774. https://doi.org/10.1038/nri3070
43. Drevets DA, Dillon MJ, Schawang JE, Stoner JA, Leenen PJM. 2010. IFN-γ triggers CCR2-independent monocyte entry into the brain during systemic infection by virulent *Listeria monocytogenes*. Brain Behav Immun 24:919–929. https://doi.org/10.1016/j.bbi.2010.02.011
44. Hess A, Axmann R, Rech J, Finzel S, Heindl C, Kreitz S, Sergeeva M, Saake M, Garcia M, Kollias G, Straub RH, Sporns O, Doerfler A, Brune K, Schett G. 2011. Blockade of TNF-α rapidly inhibits pain responses in the central nervous system. Proc Natl Acad Sci U S A 108:3731–3736. https://doi.org/10.1073/pnas.1011774108
45. Kwiatkowski K, Pawlik K, Ciapała K, Piotrowska A, Makuch W, Mika J. 2020. Bidirectional action of cenicriviroc, a CCR2/CCR5 antagonist, results in alleviation of pain-related behaviors and potentiation of opioid analgesia in rats with peripheral neuropathy. Front Immunol 11:615327. https://doi.org/10.3389/fimmu.2020.615327
46. Longobardi L, Temple JD, Tagliafierro L, Willcockson H, Esposito A, D'Onofrio N, Stein E, Li T, Myers TJ, Ozkan H, Balestrieri ML, Ulici V, Loeser RF, Spagnoli A. 2017. Role of the C-C chemokine receptor-2 in a murine model of injury-induced osteoarthritis. Osteoarthritis Cartilage 25:914–925. https://doi.org/10.1016/j.joca.2016.11.004
47. Bengue M, Ferraris P, Baronti C, Diagne CT, Talignani L, Wichit S, Liegeois F, Bisbal C, Nougairède A, Missé D. 2019. Mayaro virus infects human chondrocytes and induces the expression of arthritis-related genes associated with joint degradation. Viruses 11:797. https://doi.org/10.3390/v11090797
48. Phuklia W, Kasisith J, Modhiran N, Rodpai E, Thannagith M, Thongsakulprasert T, Smith DR, Ubol S. 2013. Osteoclastogenesis induced by CHIKV-infected fibroblast-like synoviocytes: a possible interplay between synoviocytes and monocytes/macrophages in CHIKV-induced arthralgia/arthritis. Virus Res 177:179–188. https://doi.org/10.1016/j.virusres.2013.08.011
49. Ponzetti M, Rucci N. 2019. Updates on osteoimmunology: what's new on the cross-talk between bone and immune system. Front Endocrinol (Lausanne) 10:236. https://doi.org/10.3389/fendo.2019.00236
50. Kudo O, Sabokbar A, Pocock A, Itonaga I, Fujikawa Y, Athanasou NA. 2003. Interleukin-6 and interleukin-11 support human osteoclast formation by a RANKL-independent mechanism. Bone 32:1–7. https://doi.org/10.1016/s8756-3282(02)00915-8
51. Roy E, Shi W, Duan B, Reid SP, Lee B. 2020. Chikungunya virus infection impairs the function of osteogenic cells. mSphere 5:12. https://doi.org/10.1128/mSphere.00899-20
52. Amaral FA, Costa VV, Tavares LD, Sachs D, Coelho FM, Fagundes CT, Soriani FM, Silveira TN, Cunha LD, Zamboni DS, Quesniaux V, Peres RS, Cunha TM, Cunha FQ, Ryffel B, Souza DG, Teixeira MM. 2012. NLRP3 inflammasome-mediated neutrophil recruitment and hypernociception depend on leukotriene B4 in a murine model of gout. Arthritis Rheum 64:474–484. https://doi.org/10.1002/art.33355
53. Dussault A-A, Pouliot M. 2006. Rapid and simple comparison of messenger RNA levels using real-time PCR. Biol Proced Online 8:1–10. https://doi.org/10.1251/bpo114
54. Livak KJ, Schmittgen TD. 2001. Analysis of relative gene expression data using real-time quantitative PCR and the 2−ΔΔCT method. Methods 25:402–408. https://doi.org/10.1006/meth.2001.1262
55. Krohn-Grimberghe M, Mitchell MJ, Schloss MJ, Khan OF, Courties G, Guimaraes PPG, Rohde D, Cremer S, Kowalski PS, Sun Y, Tan M, Webster J, Wang K, Iwamoto Y, Schmidt SP, Wojtkiewicz GR, Nayar R, Frodermann V, Hulsmans M, Chung A, Hoyer FF, Swirski FK, Langer R, Anderson DG, Nahrendorf M. 2020. Nanoparticle-encapsulated siRNAs for gene silencing in the haematopoietic stem-cell niche. Nat Biomed Eng 4:1076–1089. https://doi.org/10.1038/s41551-020-00623-7